

THESIS

INACTIVATION OF *Mycobacterium tuberculosis* FOR SAFE USE OUTSIDE OF THE BSL-3
LABORATORY

Submitted by

Jackson Watkins

Department of Microbiology, Immunology and Pathology

In partial fulfillment of the requirements

For the Degree of Master of Science

Colorado State University

Fort Collins, Colorado

Fall 2020

Master's Committee:

Advisor: Karen Dobos

Raymond Goodrich
Richard Slayden
Ed Hall

Copyright by Jackson Watkins 2020

All Rights Reserved

ABSTRACT

INACTIVATION OF *Mycobacterium tuberculosis* FOR SAFE USE OUTSIDE OF THE BSL-3 LABORATORY

Techniques for pathogen inactivation have been long employed by research laboratories to help ease the financial, physical, and health strains associated with (A)BSL-3 work. While robust protocols exist for many of these techniques, there are many holes in research associated with characterization of damage to treated organisms, and standardized methods for comparative analysis of successful sterilization. The work in this thesis aimed to develop methods to better understand current techniques of inactivation. At the same time, it also aimed to characterize the limitations of both a novel approach to inactivation, as well as the pathogenic models we commonly use for infectious disease research. We accomplished this by first developing a D₁₀ value and standardized curve to describe inactivation of *Mycobacterium tuberculosis* by traditional cesium irradiation techniques. D₁₀ modeling is a stepping stone for comparative analysis of organisms to one another, and also maintains calibration potential to measure radioactive source decay over time. We then focused on the effect of riboflavin photochemistry on *Mycobacterium smegmatis* as a model for *Mtb* grown from large-scale culture. We demonstrated the potential for *M. smegmatis* to enter a viable but non-culturable state, as well as potential reluctance to readily uptake exogenous riboflavin, making it uniquely resistant to this specific method of photosensitizer damage. Characterization of damage to *M. smegmatis* through propidium iodide flow cytometry assays, and 8-oxoguanosine detection assays, also offered insight into the limitations of *M. smegmatis* as a model for *Mtb*.

ACKNOWLEDGEMENTS

Thank you first and foremost to Dr. Karen Dobos for supporting me financially and emotionally through not only this project, but the last seven years of my life which I have spent in her lab. Special thanks to Terumo BCT and Ray Goodrich who provided much of the Mirasol specific materials for these experiments. Thank you to Lindsay Hartson for helping design the 8-oxo-guanisine assays, as well as for her valuable insight and technical skill for Mirasol operations. Chris Allen and Marcela Henao Tamayo were essential for the development of our flow assays, and Phillip Knabenbaur for his help in designing our dose-response protocols.

I acknowledge that the land this University is situated on was acquired through the forced removal, genocide, and continuing colonization of the Arapahoe, Cheyenne and Ute nations and peoples. Much of Colorado was stolen through coerced cession of land belonging to indigenous peoples, which was further recognized as theirs legally by the United States government through the 1851 Fort Laramie Treaty. Most often, acquisition of this land occurred through violent confrontation. As a land grant institution, I also acknowledge that Colorado State University must prioritize projects and further actions which benefit the original stewards of this land, by both acknowledging our past, and working with indigenous peoples to meet their needs moving forward, without excuse.

TABLE OF CONTENTS

ABSTRACT.....	ii
ACKNOWLEDGEMENTS.....	iii
CHAPTER 1: INTRODUCTION	1
CHAPTER 2: CESIUM-137 SOURCE GAMMA-IRRADIATION.....	10
CHAPTER 3: MIRASOL INACTIVATION OF <i>M. SMEGMATIS</i> AS A MODEL FOR <i>MTB</i> ..	21
CHAPTER 4: CHARACTERIZING MIRASOL DAMAGE TO <i>M. smegmatis</i>	34
CHAPTER 5: CONCLUDING REMARKS AND FUTURE DIRECTIONS	47
REFERENCES	51
APPENDIX A.....	60
APPENDIX B	61
APPENDIX C	62

CHAPTER 1: INTRODUCTION

Inactivated Pathogens

Human risk group-3 (HRG-3) pathogens maintain clinical and ecological interest because of their ability to infect hosts and manifest diseases with high mortality rates. While there remains a strong clinical desire to study these pathogens for the advancement of human health, proper protection of those who work with these organisms is challenged by financial and mechanical barriers¹. For researchers to mitigate risk of laboratory acquired infections (LAI), respiratory pathogen work requires high-containment settings such as biosafety level-3 (BSL-3) laboratories for safe growth and manipulation². While these laboratories are most ideal for protection of both researchers and their communities, the aforementioned financial burdens make them nearly infeasible in some parts of the world⁵. It too must be acknowledged that any facility conducting work with deadly and contagious pathogens maintains some risk of spill-over from the laboratory setting into the communities where the research is situated^{8,13}. Each of these barriers to high-risk pathogen research, are amplified in countries which are resource-poor, wherein those same countries find themselves most susceptible to outbreaks^{1,5,6}. And though these barriers are certainly amplified in resource-poor communities, they are present even in communities with ample means to finance research, as facilities require maintenance and extensive training, while having a slight but non-zero risk of infection to researchers and subsequently, their communities⁷.

Inactivation Techniques

A wide variety of inactivation techniques have been developed for the purpose of rendering pathogens non-viable, while also leaving cell constituents, media, or suspension of interest intact⁴⁸. Such techniques for sterilization find utility in food and water-system safety⁴⁵⁻

⁴⁷, purification of transfusion and plasma-derived products^{53,55,56}, and laboratory applications such as diagnostics and basic science research^{48,54}. In the context of the latter, inactivation techniques are beneficial for the continuing safety of those conducting research with biological hazards. Our interest in the application of inactivation techniques, stems from a desire to work with pathogens and their constituents outside of BSL-3 containment, while working with inactivated material that maintains much of its structural and enzymatic characteristics. However, each technique for inactivation comes with both positive and negative attributes, and a one-size-fits-all approach has not been fully developed.

Heat inactivation of pathogens is most common in food and water safety, but also utilized in laboratory settings⁴⁵⁻⁴⁷. High heat treatment, especially beyond 95°C, is profoundly effective at inactivation of not only pathogens, but resilient spores formed by treatment resistant organisms⁴⁵. Lower heat treatments have more variable in efficacy of inactivation, but adequate temperatures to inactivate are described in the literature for many common laboratory pathogens^{46,47}. As a result, information on D₁₀ values (commonly referred to as D-values in the literature; the treatment parameters required to reduce bacterial or viral load by 90%) is easily accessible. Comparison of these values has led to robust relative measurements of heat resistance across microorganisms. However, downstream application for heat-treated pathogens is minimal, as heat causes widespread damage to proteins, lipids, and many cellular components⁴⁵. While our lab utilizes heat for DNA preparations, due to high heat requirements for DNA denaturation, we seldom use it in other contexts where heat may disturb downstream analysis of protein secondary and tertiary structure, cellular component integrity, or normal lipid and enzyme function. This technique, despite its incredible utility in sterilizing or reducing microbial load in food and water products, maintains limited practical use in the laboratory setting.

Lipid solvents have also been well described for bacterial and viral inactivation^{55,56}. Solvents like chloroform, hexane and ethyl-ether are useful for isolation of cellular DNA, lipids, and membrane proteins. In low concentrations, chloroform has even been used to reduce pathogenic load in plasma products⁵⁶, though due to the toxicity and hazards associated with solvents, can't be realistically upscaled to large concentrations of cells, without generating proportionally large amounts of hazardous waste. Besides the generation of toxic byproduct, chloroform is also only useful for enveloped viruses, or organisms with lipid membranes, made soluble by organic solvents. Lipid solvents are so ineffective at inactivating non-enveloped viruses, that treatment with chloroform and subsequent plaque assays have been used by virologists to classify newly discovered viruses as either enveloped, or non-enveloped⁵⁶.

Cesium-Source Gamma-Irradiation

To address the barriers to research, we and others use cesium-source (Cs-137) gamma-irradiation to inactivate pathogenic organisms for safe use outside of the BSL-3 laboratory setting. Gamma-irradiation has been crucially effective because of its ability to specifically inactivate pathogenic organisms⁸⁻¹² through long described mechanisms of oxidative stress to cellular DNA^{11,12}. Though evidence supports that some damage may also occur within DNA repair machinery¹², cells remain mostly in tact due to the specificity of damage, maintaining much of their structural and component integrity, as well as metabolic function⁶³. This has been particularly useful in our laboratory for shipment and applications such as subcellular fractionation, protein and lipoglycan purification, and associated proteomics and metabolomics analysis. Elsewhere, gamma-irradiation of HRG-3 pathogens has allowed for significant advancements in research. These advancements include but are not limited to steps forward in

diagnostic techniques^{14,15}, vaccine production^{16,17,18}, and basic research immunology¹⁸, which all have implications for human health in the face of epidemics and spread of HRG-3 pathogens.

It should however be noted that accidental release of inadequately irradiated organisms has been documented as recently as the 2015 Dugway incident^{36,37,71}. This particular event, where samples containing live anthrax spores were incompletely irradiated and shipped out of the contained environment, posed a significant risk to both researchers and public health³⁶. The event lead to the temporary closure of nine biodefense laboratories, and 41 potential exposures to live samples^{36,37}. Such incidents, especially in such recent history, demonstrate both a need for strict protocols when dealing with deadly organisms, and a continuing interest in validating irradiation devices that we rely on to properly inactivate harmful pathogens. More recently, our lab experienced alamar blue dye positive results from samples which had been treated at the approved lethal dose of gamma-irradiation. Alamar blue dye viability assays are used in our lab to qualify inactivated pathogens and confirm complete inactivation of cells before shipment outside of the BSL-3 facility. Naturally, seeing positive results from treated cells, was concerning. Additional concerns exist as well, including costs of operation, the incredible danger of the source to humans if exposed, and concerns about radiological decay, and effectivity of a decaying source over time.

To address these recent concerns, we aim to both improve understanding of our current inactivation protocols, while also looking into the plausibility of new methods for inactivation. Additionally, this work interrogates the use of *Mycobacterium smegmatis* (*M. smegmatis*) as a model organism for *Mtb*, particularly in the context of UV photochemical inactivation with riboflavin as photosensitizing agent. This will speak to a greater concern, in understanding how near-neighbor organisms may fail to adequately represent human pathogens.

The first aim was the development of a methodology and protocol for biological calibration of a Cs-137 gamma-irradiator, based on its ability to inactivate *Mycobacterium tuberculosis* (*Mtb*) at purported Megarad (Mrad) doses. This protocol addressed issues that exist in regards to ambiguity in measuring actual radiological dose to samples in the irradiator, through traditional methods like Fricke⁷², ion chamber⁷³, and thermoluminescent dosimetry⁷⁴. An in-house study conducted at CSU demonstrated variability across, and even within dosimetric methods¹⁹. Furthermore, even if these calibration methods were robust, they would give little insight into how a given dose realistically affects pathogen viability. That is to say, no direct data existed before this study to demonstrate directly, how dose affects viability markers like colony forming units (CFU) for *Mtb* or *M. smegmatis*. Since Cs-137 has a relatively short half-life of around 30 years, we also desired a biologically relevant baseline, which can be used in the future to demonstrate how half-life decay of the Cs-137 source affects viability of *Mtb* at given doses. Thus, we generated a dose-response curve based on increasing Mrad doses delivered to *Mtb* standards, and the consequent decreases in CFU/ml and cellular respiration. As a result, we generated a highly reproducible dose-response curve, which gave us a method to directly calibrate the purported doses to CFU/ml reduction. From this data, we also calculated a decimal reduction (D_{10}) value, that being the Mrad dose required to reduce CFU/ml by one log, or 90%⁶³. Our studies have led to the generation of a highly reproducible D_{10} curve and accompanying method which can be implemented broadly across our laboratories and others. We demonstrated the possibility to robustly calibrate Mrad doses from a decaying radioactive source over time, to the reduction of CFU from a given sample space. This work was crucial in addressing seemingly arbitrary doses, by giving exact dose-response data in terms of CFU/ml, a biologically relevant measure of cell division.

Mirasol Pathogen Reduction Technology

As previously mentioned, even with robust calibration methods, downsides such as cost and safety remain as concerning downsides to inactivation by Cs-137 gamma-irradiation. For our next aim, we sought to investigate an alternative, by characterizing the capabilities of Mirasol Pathogen Reduction Technology (MPRT) to inactivate cell pellets from large-scale culture. MPRT has previously been demonstrated to completely inactivate pathogens in human blood^{20,21,22}, currently making it a useful tool in hospitals for quality control during blood transfusions^{20,21}. Additional studies have also demonstrated complete inactivation and extensive DNA damage in 8 log cultures of *Escherichia coli* (*E. coli*)²³. The process of inactivation involves a photosensitizing reaction between ultraviolet (UV) light and riboflavin, which causes 8-oxo-guanosine modifications at guanosine DNA nucleosides. Irreversible double-strand breaks in cellular DNA are characteristic biomarkers of this type of damage^{20,23}. Similar specificity of damage is observed as in gamma-irradiation, making the option attractive for our purposes.

Because of its clinical efficacy, we predicted that the MPRT would be a useful tool for inactivating large pellets of pathogenic *Mtb*, as a replacement for the cesium-source gamma-irradiation. By measuring reduction in colony forming units (CFU) at increasing UV doses, we characterized the damage done to the *Mtb* model organism, *M. smegmatis*, by the MPRT. We found that while a significant reduction in replicating *M. smegmatis* cells could be consistently achieved over multiple replicates, surviving populations of cells remained, even after high doses of UV light.

Characterization of Damage to M. smegmatis

This resistance to treatment led us to our third aim, characterizing the damage to *M. smegmatis*. Gel images indicate that little to no shearing occurred within the DNA of treated

cells, despite a nearly 6 log reduction in CFU/ml. Fragmented DNA treated with SAU-3 restriction enzyme, demonstrated a similar lack of shearing in *M. smegmatis* DNA. Shearing of cellular DNA is a well-documented biomarker of successful type one and two photosensitizer damage^{20,21}. It is hypothesized that the damage occurs as a response to failure of DNA polymerase to read 8-oxo-guanosine bases, which form in a response to photosensitization. Consequently, cells enter an apoptosis-like programmed cell death, characterized first by degradation of cellular DNA^{20,23}. We also expected to see shearing of DNA from oxygen radical formation as a result of the photochemistry between riboflavin and UV light.

Our results from looking at *M. smegmatis* DNA lead us to hypothesize that riboflavin was not being adequately delivered to cells through uptake from exogenous sources. Preliminary work done by our collaborators with riboflavin synthesis gene knockout mutants demonstrated the difficulty of *M. smegmatis* survival without endogenous mechanisms for riboflavin synthesis (data not shown). Reactivation of knockout mutants required a significantly higher concentration of riboflavin, compared to *Mtb*, despite both relying on endogenous synthesis of riboflavin for survival. This work may imply that riboflavin uptake is poorer in *M. smegmatis* than *Mtb*. This may also imply a broader issue with photosensitizer inactivation by MPRT when dealing with organisms which synthesize riboflavin endogenously rather than relying on exogenous uptake.

Due to the possibility of decreases in photochemical activity, we were also concerned that much of the loss in culturable cells could be attributed to UV-induced viable but nonculturable cells (VBNCs). The phenomenon of VBNCs induced by extracellular stress is well described in *Mycobacterium spp.*^{40,41} as well many other bacterial species^{38,39}. VBNCs are characterized as cells which have lost their ability to grow in media, while maintaining structural integrity, some metabolic function, cell wall integrity, protein function, and so on³⁸⁻⁴¹. More concerning, VBNCs

are associated with reactivation and maintained virulence in pathogenic organisms. UV-induction of the VBNC state has also been well described^{38,39}, being first observed as early as 1994⁴². The VBNC dormancy state has also been associated with increased resistance to traditional inactivation methods such as antibiotics, heat, ethanol, and oxidative stress^{38,43}.

To identify VBNCs in treated samples, we used Propidium Iodide (PI) staining and flow cytometry to quantify programmed cell death, as well as an 8-oxo-guanosine detection assay to measure the extent of damage as a biomarker for successful treatment. PI stain, which only enters cells which have permeabilized membranes, is used as an indicator of cell viability⁴⁴. Unsuccessful PI uptake indicates that cells have an intact membrane, and comparing to a control group allowed us to compare rates of capturability to rates of membrane permeability. 8-oxo-guanosine detection assays were measured in comparison to a standard curve, and gave insight into the photochemical activity that was occurring in cells treated by MPRT.

Ultimately, we found through our studies that neither 8-oxo-guanosine formation, nor programmed cell death, were occurring at the rates seen in controls. This was determined through direct colorimetric detection assays, and flow cytometry. Despite the significant reduction in replicating cells as indicated by CFU/ml counts, the membranes of treated cells had not been permeabilized to the extent of their MIC₉₉ moxifloxacin treated controls. Another biomarker of successful photosensitizer treatment, formation of 8-oxo-guanosine modified bases, was absent from treated cells even when those same samples had significant reductions in replicating cells.

This thesis set out to test the hypothesis that MPRT would successfully inactivate *M. smegmatis* from large-scale culture. This was to be used as a model for the development of a protocol for *Mtb* from large-scale culture. Our studies demonstrated, first and foremost, that inactivation of the model organism was unachievable, even at treatment high doses, and with

some doses that were consequently successful for complete inactivation of *Mtb*. In characterizing the damage to treated *M. smegmatis*, we also discovered strong evidence to suggest that MPRT-treated *M. smegmatis* was entering a VBNC state, which has been previously correlated with increased resistance to a variety of other inactivation methods. Biomarkers, such as maintained cell wall integrity in non-culturable samples, and lack of distinct damage to DNA supported this new hypothesis. Even so, we were able to successfully inactivate *Mtb* at doses which did not successfully inactivate *M. smegmatis*. Future work should focus on further describing the VBNC hypothesis, in both *Mtb* and *M. smegmatis*. Initial data and further discussion regarding future studies, are expanded on in the concluding remarks of this thesis.

CHAPTER 2: CESIUM-137 SOURCE GAMMA-IRRADIATION

Chapter 2 Introduction

The accidental release of respiratory pathogens into an improperly contained environment could pose a significant risk to community and global public health^{3,4}. Our lab received samples of *Mtb* which had been irradiated at the standard dose of 2.4 Mrad, previously assumed to be twice the effective dose for lethal inactivation of cell pellets from large-scale culture. However, while conducting alamar blue dye viability assays for quality control confirmation of inactivation, we discovered alamar blue dye positive samples, indicating the possibility of live cells in our irradiated pellet.

Subsequent work was conducted¹⁹ to calibrate the device based on a simplified dosimetry model which generated an expected dose rate of $3.25 \text{ Gy} \cdot \text{min}^{-1}$ for the cesium source¹⁹. Fricke dosimetry gave a dose rate result of $5.2 \text{ Gy} \cdot \text{min}^{-1}$ (Supplementary Figure 2A), ion chamber dosimetry an average rate of $7.19 \text{ Gy} \cdot \text{min}^{-1}$ (Supplementary Figure 2B), and thermoluminescent dosimetry (TLD) and average rate of $7.56 \text{ Gy} \cdot \text{min}^{-1}$ (Supplementary Figure 2C). Further, there seemed to be variation in dose rate based on position in the device, as indicated by data collected by ion chamber and TLD. Because of the variation between each of the calibration methods, as well as the significant difference from the expected calculated rate, Brandl and Bell recommended that a particular value of calibration should not necessarily be universally applied and emphasized, as variation exists between methods, and high dose rate environments (like ours) are difficult to calibrate outright. Additionally, there seemed to exist variation between positions in the irradiation chamber, that ought to be investigated.

Alamar blue dye contains resazurin, a blue compound which is reduced to the pink fluorescent resorufin when its oxygen is used for cellular respiration as a precursor for cellular metabolic activity (Figure 1). Since resazurin has a relatively high reduction potential of +380mV at pH=7, 25°C, it easily accepts electrons during cellular respiration, from several metabolic cofactors such as NADH and FADH^{24,25}. This dye is useful for a variety of applications, such as microbial detection assays in food contamination QC, and popularly as a measure of cell viability in cells treated with test compounds²⁴. This assay has been particularly popular in measuring viability of *Mycobacteria* treated with a wide range of compounds²⁴. That said, it has been recently demonstrated in *Mtb* that alamar blue assays have a wider range of sensitivity and specificity in accurate drug susceptibility testing, compared to other viability assays such as nitrate reductase assays, and MGIT 960²⁶. This may more broadly imply, that there exists a higher probability of both false negative, and false positive results from alamar blue assays.

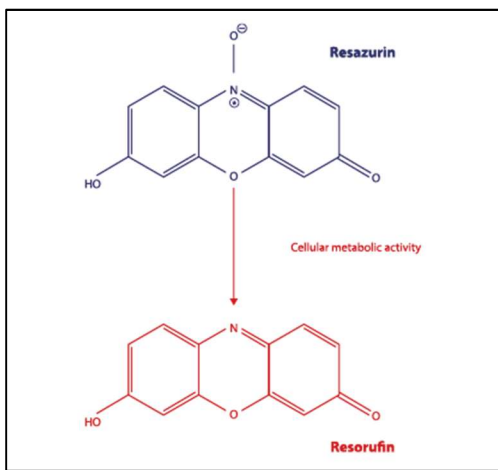


Figure 1 (above). Resazurin reduction mediated by metabolic cofactors such as NADH and FADH. Image copyright Canvax Biotech, S.L. C/Astrónoma Cecilia Payne. Edif. Canvax. 14014 Córdoba, Spain.

It is possible that our previous alamar blue results are falsely positive, induced by contamination of media. However, this sparked a greater interest for our lab, in understanding how devices are calibrated for inactivation of pathogens. Despite having a few methods for calibration such as the previously mentioned Fricke, ion chamber, and TLD dosimetric methods, none provided the ontological connection between doses delivered to samples, and actual markers of loss in cell viability. No research or standard currently exists, to quantify Cs-137 reduction in *Mtb* viability. Furthermore, considering the 30 year half-life decay rate of Cs-137, a standard methodology describing how to describe reduction in viability relative to Mrad delivered, will be useful in the future for comparative studies demonstrating how, for example, a quarter half life affects efficiency of a given Mrad dose and consequent reduction in sample viability. We were effectively in the dark about how radiological decay was altering the efficiency of the Cs-137 source to reduce viable cells; We knew that our standard 2.4 Mrad dose was historically sufficient for complete inactivation, but had no actual dose-response representing lower doses, or a D_{10} value. For this reason comparative studies were impossible, causing the Mrad dose delivered to be effectively arbitrary in the context of understanding how dose correlates to inactivation.

D_{10} modeling of inactivation offers a mathematically robust, and standardized method for comparing success of inactivation methods^{63,64}. Such modeling has been important in describing pathogen susceptibility to both cesium and cobalt irradiation⁶³⁻⁶⁷, with methods for generating D_{10} models dating back nearly 50 years⁶⁷. While they remain important for standardizing inactivation by irradiation, a robust study on *Mtb* D_{10} modeling, to our knowledge, has not been undertaken.

Thus, from the work completed in this chapter, we successfully generated a dose response curve and D_{10} value which can be used as a biologically pertinent method for calibration of half-life over time. Additionally, it gives insight into the susceptibility of *Mtb* to cesium-based damage, and can be valuable data for comparison to other organisms, as well as *Mtb* down the line. The reproducibility and accuracy of the curve we generated, implies that the protocol will be effective elsewhere. Theoretically, the methodology in this chapter can be applied elsewhere, in different facilities, with substantial success.

Methods

Sample Preparation

Working stocks of *Mtb* were generated by culture on 7H11 media incubated at 37°C. After four weeks of growth, plates were transferred to GAS media + 20% glycerol, and stirred on a magnetic stir plate for another 4-6 days. 1 ml aliquots were transferred to 1ml cryovials and stored at -80°C until use. Ninety working stocks were thawed and distributed three each into 30 5x5 fibreboard cryogenic freezing boxes (VWR) in three positions (top left, true center, and bottom right). The remaining 22 positions that did not contain cells, were filled with 1.2 ml cryovials containing 1 ml of GAS media + 20% glycerol. The boxes were labeled for treatment, four boxes for each of our 6 gamma-irradiated treatment doses. Additionally, each treatment group would have a “maze control” box intended to be placed within a few feet of the irradiator for the duration of respective treatments. The four remaining vials were kept at -80°C, to be used as positive controls in CFU and Alamar Blue experiments.

Gamma-Irradiation

Boxes were wrapped within three autoclave bags, to ensure triple-containment of potentially viable pathogenic organism. While each of the four boxes per dose were treated, a maze control remained in the room for the duration of the treatment. Maze controls, in this context, are control vials which are left in the room while the irradiation device is being used, to control for room and vial conditions on bacterial growth. It acts then as a negative control, as well as a potential indicator of environmental contamination from the irradiation device. During treatment, boxes were placed on the top shelf of a JL Shepherd Model 81-14 sealed source Cs-137 Irradiator. The top shelf from the cesium source was used. Four boxes each were treated at the following doses: 0.001 Mrad, 0.005 Mrad, 0.010 Mrad, 0.050 Mrad, 0.100 Mrad, and 0.150 Mrad. Boxes were transported back to the BSL-3 laboratory, and frozen at -80°C. Though we expected some loss from an additional freeze-thaw, a post-treatment freeze-thaw is consistent with in-house protocol for *Mtb* inactivation.

CFU Plating and Counts

Boxes were thawed, and the contents each sample vial were transferred to individual 1.7 ml microcentrifuge tubes. Each tube was spun on a microcentrifuge at 3.75K for 10 minutes, and the supernatant was removed after centrifugation. 1 ml of PBS was added to each tube, followed by an additional centrifugation at 3.75K for 10 minutes. PBS supernatant was removed, and cells were resuspended in 1 ml of 7H9 media with OADC and 0.05% Tween 80. Each tube was placed in an ultra-sonic water bath and sonicated 30 seconds on, and 30 seconds off, three times. In a 24-well sterile plate (VWR), each of the sonicated samples were diluted out in a 1:10 series to the 10^{-6} dilution. Dilutions were made with 100 μ l of sample in 900 μ l of 7H9 media with OADC and 0.05% Tween 80. From all maze controls, and all treated samples up to 0.100 Mrad, 100 μ l of the highest three dilutions (10^{-4} , 10^{-5} , 10^{-6}) were plated in triplicate on 7H11 media (Dobos

Lab SOP: M009.2) in quad petri dishes (VWR). For 0.100 Mrad treated samples, excluding maze controls, 10^{-2} , 10^{-3} and 10^{-4} dilutions were plated in triplicate. For 0.150 Mrad treated samples, excluding maze controls, 10^{-1} , 10^{-2} and 10^{-3} dilutions were plated in triplicate. Plates were incubated at 37°C for 16 days before reading colonies. The remaining 900 µl from each sonicated sample, was transferred to its own sterile glass tube containing a sterile stir bar. Samples were placed on a stir plate for 72 hours at 37°C in preparation for Alamar blue viability testing.

Alamar Blue Viability Testing

Samples were removed from incubation and 200 µl of each was added in triplicate to a 96-well plate. Samples were read at optical density 600 (OD₆₀₀) to standardize concentration. Samples were then diluted accordingly to standardize to an OD₆₀₀ of 0.1, and serial diluted in 7H9 + OADC + 0.5% Tween media 1:10 out to an OD₆₀₀ of 0.001. 20µl of Alamar Blue dye (Invitrogen) was added to each sample well. Absorbance measurements were performed at dual wavelengths 570nm and 600nm for the 0hr timepoints. Plates were wrapped in foil, incubated at 37°C, and read at 24h and 48h timepoints. Linear regressions were applied to each series of measurements, and the slope was used for comparative analysis. Regressions were applied regardless of R²-values. Slopes of each regression were compared to their respective maze controls using non-parametric Mann-Whitney t-tests from GraphPad Prism 7.04.

Results

Linear regression model ($y = -34.69x + 8.219$) was fitted to the treatment doses affect on CFU/ml with an R²-value of 0.9941. The dose-response curve, generated as a linear regression on a log-scale y-axis, predicts a D10 value of 0.029 Mrad. That predicts then that a dose of 0.029

Mrad is necessary for a one log, or 90% reduction in CFU/ml (Figure 2C). This represents 1.2% of the total standard dose delivered to samples shipped from our laboratory.

Reduction in CFU/ml was measured with the box position parameters described in the methods. There is not a significant difference between CFU/ml reduction at any particular position, implying even distribution of irradiation (Figure 3).

Alamar Blue comparative slope analysis was used to compare general enzymatic activity and viability through reduction of Alamar Blue dye by treated cells. A significant drop in Alamar Blue dye reduction was not observed until 0.15 Mrad (Table 1), which correlates with a 5.2 log reduction in CFU/ml according to the slope generated in Figure 2. There was a significant difference between the maze control and treated sample slopes at the 0.005 Mrad treatment as well, however it was in the opposite direction. Reasons for this data are explained further in the chapter discussion.

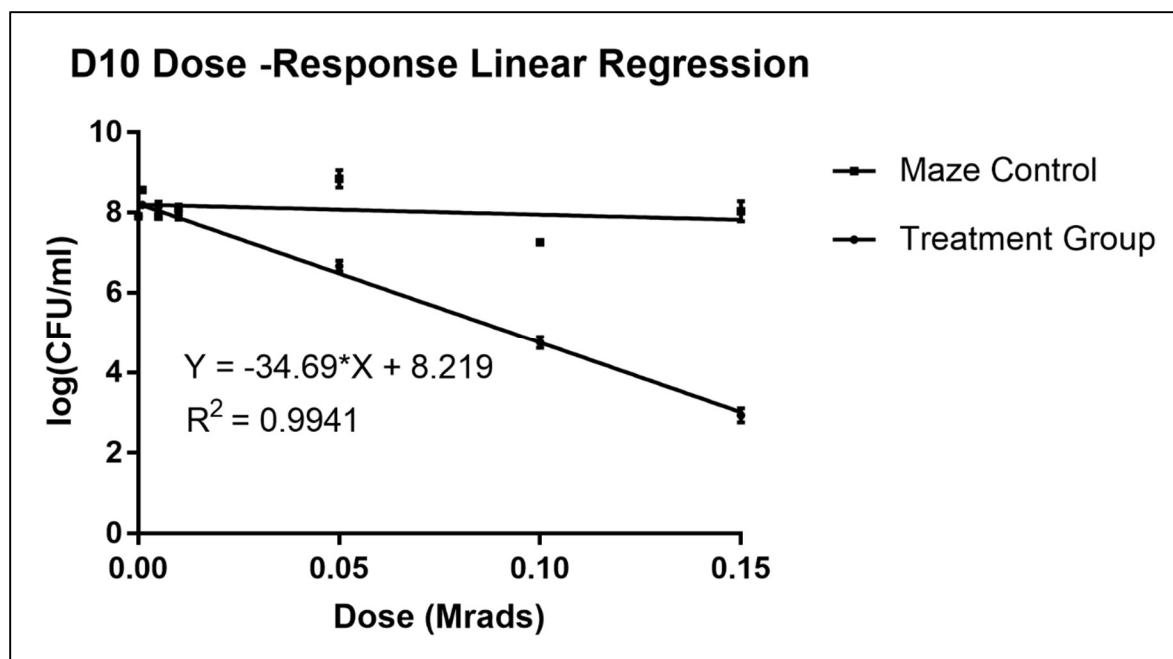


Figure 2 Viability of *Mtb* exposed to gamma-irradiation (above). *Mtb* H37Rv was exposed to increasing doses of Cs-137 gamma-irradiation and plated for CFUs on 7H11 agar. Dose Response generated based on CFU/ml after treatment, with slope and R^2 of Treatment Group given. Slope indicates D10 value of 0.029 Mrad, that being the dose which leads to 1 log, or 90% reduction in CFU/ml. Regression slope test indicates with a p-value < 0.0001 that the difference in slopes is not equal to zero, indicating a significant difference between slopes.* indicates p-value<0.05.

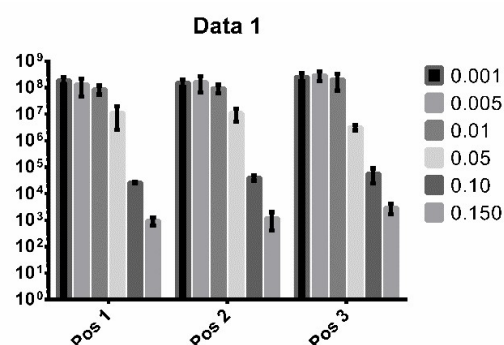


Figure 3: Position-Based Reduction of CFU/ml (above). CFU/ml measurements were collected from three different positions as described in the methods. Reduction in CFU to each of the three positions across increasing treatment was tested. No significant difference in reduction at any timepoint between positions was observed.

Table 1: Alamar Blue Slopes of Reduction (below). Alamar Blue dye assays were performed at 0h, 24h, and 48h timepoints, and slopes were applied to changes in absorbance as measured by 570nm over 600nm. Mann-Whitney nonparametric t-tests were used to compare median slopes generated in Alamar Blue dye assays, between treated samples and non-treated maze controls. ** = $p < 0.005$

Alamar Blue on Irradiated Samples			
Dose	Median Slope of Treated Sample	Median Slope of Maze Control	Mann-Whitney Significance
0.001 Mrad	0.021	0.022	ns
0.005 Mrad	0.031	0.005	**
0.01 Mrad	0.023	0.03	ns
0.05 Mrad	0.0033	0.0021	ns
0.1 Mrad	0.001	0.0013	ns
0.15 Mrad	4.35E-05	0.001	**

Chapter 2 Conclusions and Discussion

In this chapter, we have successfully developed a method for biological calibration of irradiation devices used to inactivate pathogens. Not only were the data points collected highly reproducible, but our linear regression model accounts for nearly all variance, indicating that our methods have generated a model which can be used in future experiments with a high level of confidence. Ultimately, what we have accomplished is a D10 method and model which will help us calibrate our gamma-irradiator as the Cs-137 source decays over time. This model is biologically pertinent, because calibration is termed by biological relevance, as opposed to abstracting what is relevant with Mrad or $\text{Gy} \cdot \text{min}^{-1}$ numbers which thus far, cannot be calculated on a reliable and reproducible basis¹¹. Without a biological model, Mrad doses as they decay and apply to inactivation of bacterial samples are, ambiguously applied.

A dose of 0.050 Mrad was the first in the curve to reduce cell culturing viability by at least 90%. The model indicates that a dose of 0.029 Mrad would be sufficient for a one log or

90% reduction in CFU/ml. For future calibration efforts, comparisons in CFU/ml reduction can be made on the basis that 0.029 Mrad generates a one log reduction in CFU/ml (Figure 2). Practically speaking, this means that we have a robust D10 value for future comparison, which is crucial for understanding how decay over time affects ability of the source to reduce live pathogen. Even more exciting, is that a protocol has been developed which can be easily implemented by laboratories that desire this sort of biologically relevant calibration.

Position data (Figure 3) was compelling in its demonstration that position on the irradiation device does not influence the reduction of CFU/ml that we observed. We can interpret this, because of our robust level of reproducible measurements, to imply that the Mrad dose received from our Cs-137 source is consistently distributed to the treated sample. This answers an important question of source dosimetry for our Cs-137 source gamma irradiator, by demonstrating even distribution of dose delivery by the calibration standard of CFU/ml.

Alamar Blue results indicated that significant drops in the amount of dye reduced by treated cells, do not occur until the 0.15 Mrad treatment, which correlates to an approximate 5.2 log reduction in CFU/ml as modeled in Figure 2. Previous literature has long demonstrated that a >6 log reduction in CFU/ml is necessary for confidence in inactivation of live agents⁸. Although significance was measured prior to achieving a 6 log reduction, it occurred much further down the line in treatment compared to CFU/ml counts, indicating that Alamar Blue dye is much more sensitive as an indicator of cell viability. In other words, it takes a higher dose and consequent reduction in viable cells to observe differences between treatment and control groups in Alamar Blue assays, compared to CFU assays. We did also notice a significant difference between treatment and control groups at the 0.005 Mrad dose, however it was in the opposite direction. This is expected, since the dose induces stress conditions, particularly oxidative stress, which

upregulate a number of heat shock proteins such as ACR and HSP-3, as well as KatG stress-related genes and σ -factors⁶⁹. Metabolomic and proteomic studies could be conducted in the future to further demonstrate this hypothesis. It is likely then that since the conditions created by low-dose treatment are not enough to significantly reduce (Figure 2), but still possibly generate a stress response⁶⁹, that cells are seeing increases in enzymatic activity as they respond to treatment. Future work can be done to determine exact expected reductions in Alamar Blue colorimetric changes associated with a >6 log reduction.

Future work may also focus on other biologically relevant assays, which may vary from lab to lab based on each individual standard for verifying lack of cellular activity. Additionally, this work should be reproduced regularly every 5 years, representing 1/6 the half-life of cesium, to generate a standard calibration that demonstrates the effect of decay on bacterial inactivation.

Our work in this chapter has led to a reproducible method and standard for comparative studies to study the effect of radiological decay on cell viability. However, this work has not addressed other issues with Cs-137 gamma-irradiation, such as safety and cost. For that reason, the next chapter will focus on an alternative inactivation technique, which has demonstrated to be safer and more cost-effective than gamma-irradiation.

Chapter 3 Introduction:

Inactivation by UV and riboflavin treatment has traditionally been used in hospital settings to purify blood products for transfusion into patients. This process can be mediated by Mirasol Pathogen Reduction Technology (MPRT), a device which has been demonstrated to completely inactivate pathogens in human blood²⁰⁻²². Previous studies demonstrated its usefulness for inactivating small concentrations of viral and bacterial pathogens in blood. However, despite the potential for the MPRT to inactivate bacterial pellets from large-scale culture, the technology has not been implemented in the research setting for inactivation of HRG-3 pathogens for downstream use. We aimed to translate the clinical success of the MPRT into the research setting, by inactivating bacterial pellets for widespread distribution to research laboratories.

The mechanism of damage employed by the MPRT is DNA fragmentation by oxidative radicals generated as a byproduct of the UV-riboflavin photosensitizing reaction^{27,28}. Riboflavin intercalates into the cellular DNA, at guanosine base motifs. Once riboflavin has bound to these bases, UV-B light (280-360nm) generates a photosensitizing reaction which modifies guanine to 8-oxoguanosine^{20,23}. This 8-oxoguanosine motif cannot be read by DNA polymerase and as a result cells fail to continue replication and they enter an apoptosis-like programmed cell death. UV damage alone can often be repaired by the cell, while damage caused by UV light in combination with Riboflavin has been demonstrated to cause irreparable damage in treated cells^{20,23}. This method shows promise in its ability to inactivate pathogenic organisms, without causing widespread cellular damage. Damage is restricted to the DNA, leaving the rest of the cell

intact for downstream analysis, such as lipidomic and proteomic interrogation^{22,29}. This property of the MPRT is implied to by its widespread use in hospitals, where platelet and plasma protein quality are crucial for the successful transfusion of blood from one patient to another²⁰.

The study in this chapter aimed to generate dose-response curves on bacterial cell pellets generated through current laboratory protocols for large-scale growth of *Mycobacterium* spp. *M. smegmatis* was used as a near-neighbor model organism for *Mycobacterium tuberculosis* (*Mtb*), as the MPRT had not yet been approved for use inside of the BSL-3. *M. smegmatis* has been used frequently in modern literature to model *Mtb*, helping elucidate *Mtb* molecular mechanisms, like ESX-1 secretion and DosR transcriptional regulators, factors of virulence, and host response studies⁷⁰. Near-neighbor, in the context of pathogen research then, is an organism with genomic similarity that is used outside of the BSL-3, to model HRG-3 organisms.

M. smegmatis is a BSL-1 environmental organism often used to model *Mtb*, as *M. smegmatis* poses few to no risks when manipulated. *M. smegmatis* maintains a number of genetic and metabolic similarities to *Mtb* which influenced researchers to accept it as a reasonable model organism^{30,31}. In the context of dosing studies, *M. smegmatis* and *Mtb* share many properties of drug and chemical resistance. β -lactamase inactivation and cell wall impermeability towards β -lactam antibiotics have been described in nearly all *Mycobacterium* as important for resistance against the antibiotic class³⁴. Shared efflux pump genes and proteins have been shown in both *Mtb* and *M. smegmatis* as potential mechanisms of broad antibiotic resistance^{33,34}. Highly conserved DNA repair mechanisms, non-homologous end joining, and rec-mediated homologous end joining have been shown similarly in both organisms, though it is hypothesized that *M. smegmatis* has an additional single-strand annealing pathway which it used to repair double-stranded breaks³². It is unknown how this may contribute to resistance against MPRT

inactivation, as the method is more extensive than normal double strand breaking that may occur in untreated cells.

Materials and Methods

M. smegmatis culture

1 ml of *M. smegmatis* stock suspension was inoculated on each 150mm x 15mm 7H11 agarose plates (VWR). Cells were spread for lawn growth and placed at 37°C for 72 hours. Bacterial growth from each plate was transferred to an individual Fernbach (FB) culture flask containing one liter of glycerol alanine salts (GAS) media (Dobos SOP:M001.1). The FB flasks were secured on a shaker table, set to 110 RPM at 37°C. After 72 hours, cells from each FB flask were pelleted and transferred to a pre-tared 250 ml conical tube. Tubes were weighed and frozen at -80°C until treatment.

UV treatment on riboflavin saturated cells

~30g and ~3g pellets were resuspended in 270ml of GAS media. Using a sterile tubing welder (Terumo), a 10" docking line (with a female luer end) was welded to the middle inlet tube on a Mirasol® illumination bag. The plunger was removed from a 60ml syringe and the syringe was attached to the female luer of the docking line that had been welded to the illumination bag. The syringe was secured in a three-prong clamp, attached to a stand, such that the syringe was elevated above the bag. Using a 50 ml serological pipette 270 ml of the cell slurry was transferred to the syringe, and through the tubing to each bag. 30 ml of 500µM of riboflavin was added to each bag for a final concentration of 50µM. A 3 ml syringe was used to remove 1ml from the bag, followed by a 3ml sample which was taken and frozen at -80°C for gel electrophoresis. The 1ml aliquot was added to column 1, row A of a 24-well plate. The sample

was diluted out 1:10 in GAS media, to a final 10^{-8} dilution. The bag was sealed approximately 1.5 inches above the bag entry port using a sterile tube sealer (Terumo).

For ~30g pellets, the bag was treated with 360 Joules (J) of ultraviolet (UV) light in the MPRT (Terumo). After the initial treatment, a 10" docking line was welded to the middle inlet of the bag, and a 3ml syringe was used to pull 1ml samples. Again, a 3ml sample was taken from the bag, to be frozen at -80°C . The 1ml samples were serial diluted out 1:10 in GAS media to a final 10^{-6} dilution.

The treatment process was repeated at UV doses of 720 J, 1080 J, 1440 J, 2880 J, 5760 J and 8640 J total. These were diluted out 1:10 to final dilutions of 10^{-6} , 10^{-5} , 10^{-4} , 10^{-3} , 10^{-2} and 10^{-2} respectively.

This entire UV treatment was repeated on two additional bags, to generate three biological replicates for the final dose response curve. Additionally, this process was repeated with a bag containing 150 uM riboflavin added to 210ml GAS.

For 3g pellets, both *Mtb* and *M. smegmatis* treatments were performed in duplicate at 8640 J and 17,280 J. Both were serial diluted to 10^{-2} from the original sample. 10% of *Mtb* material from each treatment bag was plated post-treatment, with pre-treatment control plating as well.

Plating for colony forming units (CFU) per ml

200ul of the following dilutions were inoculated on 100mm x 15mm 7H11 plates in triplicate: Positive Control: 10^{-6} 10^{-7} 10^{-8} dilutions (and 10^{-4} 10^{-5} 10^{-6} for 3 g pellets), 360J treated cells: 10^{-4} 10^{-5} 10^{-6} dilutions, 720J treated cells: 10^{-4} 10^{-5} 10^{-6} dilutions, 1080J treated cells: 10^{-3} 10^{-4} 10^{-5} dilutions, 1440 J treated cells: 10^{-2} 10^{-3} 10^{-4} dilutions, 2880J treated cells: 10^{-1} 10^{-2} 10^{-3} dilutions, 5760 J treated cells: Neat 10^{-1} 10^{-2} dilutions, 8640 J treated cells: Neat 10^{-1} 10^{-2}

dilutions. Inoculum was spread evenly on each plate using a sterile inoculation loop. The plates were incubated at 37°C for 72 hours. CFU were counted on each plate.

Dose-Response Curve from Surviving Colonies

Three surviving colonies from separate 7H11 plates generated from 8640J treated *M. smegmatis* cells were transferred to large 7H11 agar plates. Procedures from sections *M. smegmatis* culture and *UV treatment on riboflavin saturated cells* were then repeated on the cultures from treatment-resistant colonies to observe differences in dose-response generated curves.

Results

Our work resulted in the generation of dose-response data from CFU counts. This work was first done on *Mtb* near-neighbor *M. smegmatis*. We hypothesized that we would be able to completely inactivate cell pellets, by causing specific and irreparable damage to cellular DNA.

M. smegmatis Dose Response Data

CFU were counted from nine plates per treatment, with data collected from eight treatments (including untreated control) per experimental run, and three biological replicates total. This resulted in 27 CFU counts per treatment and 216 total CFU counts. After an input of 8640 J the three treated pellets measured 6.92, 6.89 and 6.83 log reductions in CFU/ml (Figures 4 and 5). Final bacterial concentrations were 874 CFU/ml, 611 CFU/ml, and 306 CFU/ml. Suspension in 150 uM riboflavin did not lead to significant changes in the response curve (Figure 6). After the 8640 J treatment, there was a 6.68 log reduction in CFU/ml. Colony growth morphology was noticeably altered in the higher dose treatments, with smaller colonies and flatter colony elevation (Figure 7B). Untreated colonies displayed normal colony morphology (Figure 7A). Both positive controls and treated samples demonstrated ‘irregular’ colony shape, a

specific morphology that is characteristic of *M. smegmatis* growth, and seen in many other Mycobacteria. When surviving colonies cultured from MPRT treatment were regrown and treated under similar conditions, there was no marked change in curve characteristics, and a 6.42 log reduction in culturable cells was observed (Figure 8). This number was comparable to previous curves. The K-value of the one-phase decay model was noticeably higher, however this is due to a higher starting value for Y_0 .

Mtb and M. smegmatis Comparative Reduction

Mtb and *M. smegmatis* were treated at 3g in 50 μ M riboflavin in a comparative trial, where complete reduction of colony forming units was observed in *Mtb*, where at the same treatments *M. smegmatis* could not be completely inactivated (Table 2). Non-replicating *Mtb* was also run on and Alamar Blue dye assay, and no cellular respiration was observed at either the 8,640J or 17,280J treatment, implying complete non-viability as well as non-culturability (Supplementary Figures 1A and 1B). Mycobacterial Growth Indicator Tube (MGIT) assays were run as well and determined that all but one treated *Mtb* samples were negative. This positive, which occurred in an 8,640J-treated sample, was regrown on 7H11 in 3 days, which may suggest contamination as we would not expect visible *Mtb* colonies in such a short time. *M. smegmatis* remains culturable at doses demonstrated to both render *Mtb* non-culturable, and non-viable, and so cannot be tested via Alamar Blue dye assay.

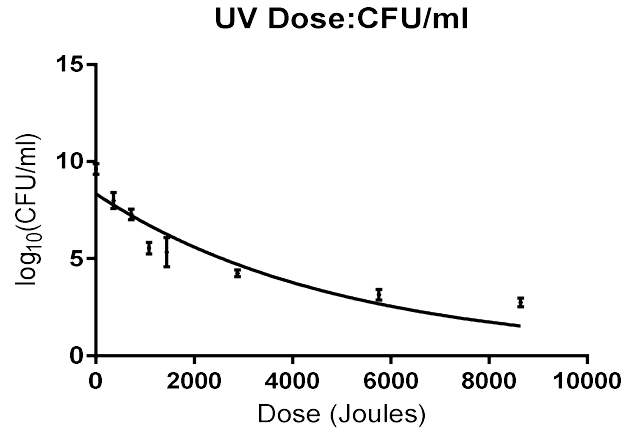


Figure 4 (above). The three biological replicates treated while suspended in 50 μ M riboflavin ($y = 8.339 * e^{-0.00022x}$). Starting bacterial concentrations were $10^{9.87}$, $10^{9.68}$ and $10^{9.31}$ CFU/ml. After complete treatment CFU/ml was reduced 6.93, 6.89 and 6.82 logs respectively, for an average of 6.88 log reduction over 8640 J total treatment.

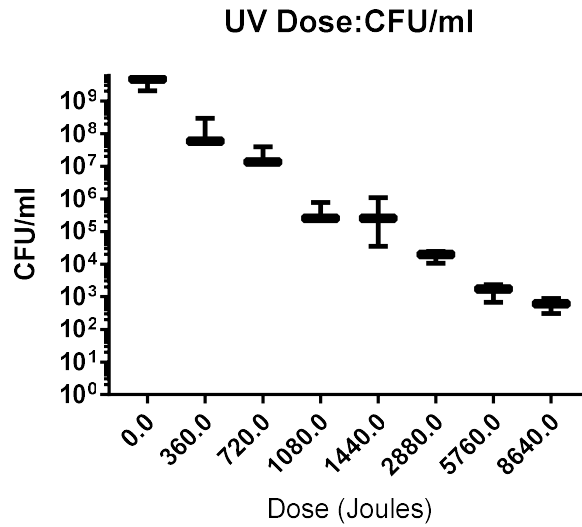


Figure 5 (above). CFU reads are consistent between biological replicates, with CFU counts at 1440 J showing relatively higher variability between CFU/ml measurements. Complete inactivation was not achieved.

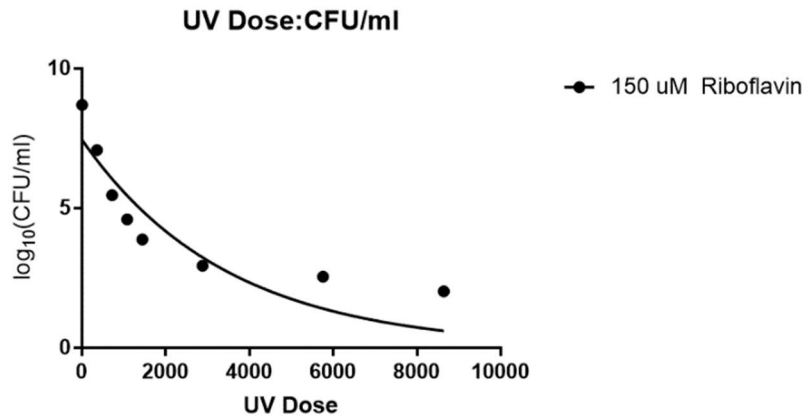
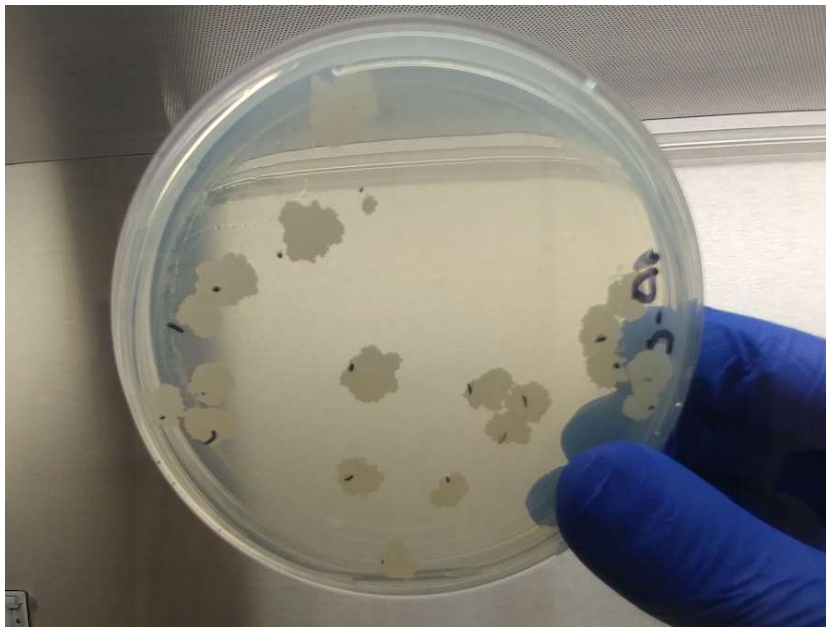


Figure 6 (above). Treatment while suspended in 150 μ M riboflavin ($y = 7.456 * e^{-0.00028x}$). Starting bacterial concentration was $10^{8.70}$ CFU/ml. After complete treatment, there was a 6.68 log reduction in CFU/ml over 8640 J total delivered.



A

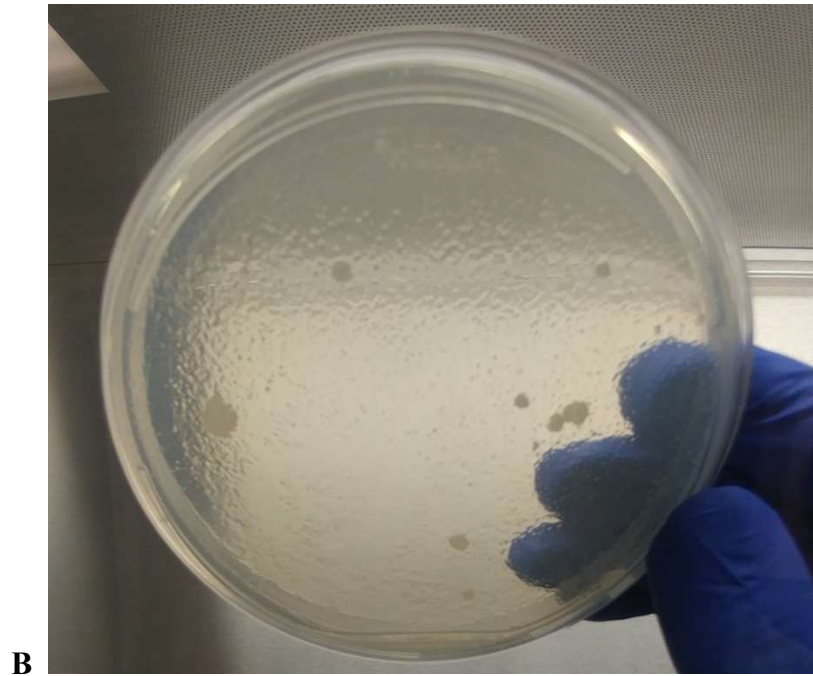


Figure 7 (above). (A) Bacterial colony growth without UV treatment in the MPRT. (B) Bacterial colony growth after 8,640 J of UV treatment with the MPRT.

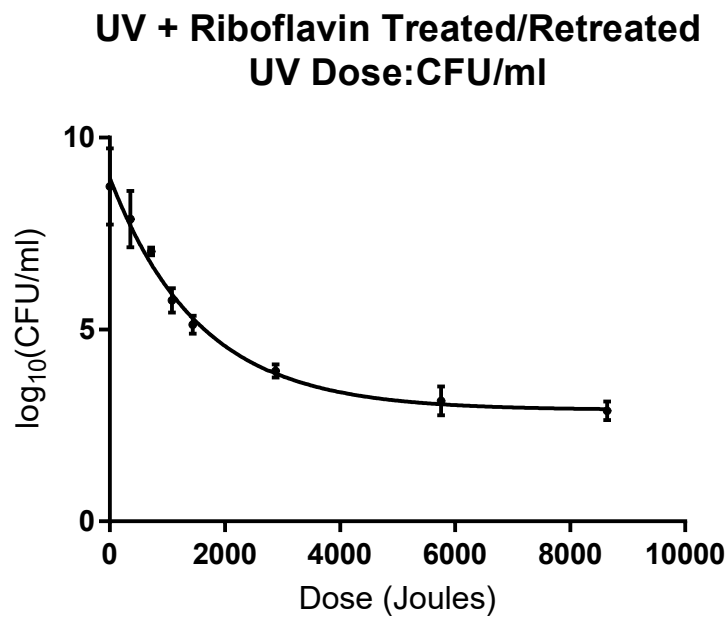


Figure 8 (above). Treatments run in duplicate from surviving colonies of MPRT treatment regrown. Treated while suspended in 50µM riboflavin ($y = 8.959 * e^{-0.00064x}$). Starting bacterial concentration was $10^{9.22}$ CFU/ml. After complete treatment, there was a 6.42 log reduction in CFU/ml over 8640 J total delivered.

Table 2 Comparative Growth Post-Treatment *Mtb* and *M. smegmatis* (above). 3g pellets were suspended and treated in a comparative study between *Mtb* and *M. smegmatis* at similar concentrations, and doses. *Mtb* was completely inactivated by the lower dose, 8,640J, as well as the highest dose of 17,280J. Surviving colonies were observed at both treatments in *M. smegmatis*. (* indicates that results come from 10% plating of total material post-treatment).

		Organism					
		<i>M. smegmatis</i>			<i>M. tuberculosis</i>		
	Replicate	Control	1	2	Control	1	2
Treatment	CFU/ml 8640J	1.46E+06	3.33	23.33	1.92E+06	0*	N/A
	CFU/ml 17280J	2.83E+06	5.00	41.67	2.95E+06	0*	N/A

Chapter 3 Conclusions and Discussion

There was clear reduction of replicating *M. smegmatis* cells at each treatment, as demonstrated through CFU/ml counts. From our initial dose-response curves, we demonstrated that there was a surviving population of *M. smegmatis* cells that grew at consistent rates after UV doses beyond 5760 J (Figure 5). Log reduction in cell growth plateaued after the 5760 J treatment. By increasing riboflavin concentration to 150µM, we hoped to demonstrate that we were experiencing concentrations of riboflavin which were too little to properly saturate cells. The curve generated with higher concentrations of riboflavin when treated with similar doses of UV light, did not increase efficacy in cell reduction caused by the MPRT (Figure 6). This indicated to us that riboflavin concentration was not a limiting factor in bacterial inactivation. This does make sense based on the literature which has demonstrated that 8 log cells of *E. coli* can be inactivated with 150 µM riboflavin²³. And although it has been demonstrated previously that *E. coli* is more susceptible to UV damage than some *Mycobacterium spp.*³⁵, photosensitizer specific damage was shown to have caused extensive death compared to UV alone in the

aforementioned *E. coli* study. Further, while we showed that a significant reduction in replicating cells could be achieved (Figure 4 and 5), a population of cells were able to survive, even at UV doses predicted to completely kill them. Colony morphology changed drastically after treatment, and *M. smegmatis* did not maintain its typical rough phenotype, treated colonies were round and smooth compared to the untreated colonies (Figure 7). Even in early S-phase, *M. smegmatis* appears rough, though the phenotype for colony shape in treated samples is consistent with early growth of the organism. This implies that surviving cells are not growing normally, indicating that damage has occurred in surviving cells. For this reason, we investigated if cultures grown from these colonies were immediately resistant to UV-riboflavin mediated killing because of an intrinsic mutation, or if they would be more susceptible to a second round of MPRT dosing due to a loss of fitness caused by exposure. Our results did not support either conjecture, as cultures from these post-treatment isolated colonies showed similar rates of inactivation to parental cells, and almost the exact same log reduction (Figure 8). Since there was no difference in kinetics between original and surviving cells during treatment, we hypothesized that mechanical barriers to cell aggregation inhibited killing. However, when treating with a ten-fold dilution, even at doses and riboflavin concentrations which effectively killed *Mtb*, we were still able to isolate surviving *M. smegmatis* colonies (Table 2).

In summary, our data showed that cells rendered non-viable with a consistent 6 – 7 log reduction, but never sufficiently enough to completely render *M. smegmatis* non-culturable, which would require an approximate 8 log reduction in colony forming units. This pattern was observed even at doses which were demonstrated to render *Mtb* both non-culturable on CFU plates, but also non-viable as indicated by Alamar Blue viability testing and Mycobacterial Growth Indicator Tube (MGIT) (Supplementary Figure 3). Survival of *M. smegmatis* colonies

was not due to mutations of mechanical barriers, however, may be due to differences in riboflavin uptake between *Mtb* and its model organism *M. smegmatis*, a hypothesis generated based on what we observed, as well as preliminary data from collaborators (Unpublished communication, Laboratory of DRS. Valerie Mizrahi and Digby Warner; University of Capetown).

Further work will be done to demonstrate whether there are biomarkers for photosensitizing damage in our treated *M. smegmatis* cells. Initial studies are described in the following chapter through analysis of DNA and PI uptake, to show whether or not the reduction in cells we observed in *M. smegmatis*, was in fact due to photosensitization. UV damage alone will also render cells non-replicable on culture media, so it is crucial to understand the kind of damage that is occurring in our treated cells.

The physiology of *Mycobacterium* may be a limiting factor in this work. The Mirasol technology was not designed for large-scale inactivation, even after diluting cells significantly. Although similar treatments have been done with *E. coli*, and some viruses, there are significant differences in physiology between each of those organisms which may alter how effective treatment is. A surfactant may help to achieve full inactivation, however adding such reagents limits the use of this biomass for downstream applications. Furthermore, we would not expect such consistent reduction in culturable biomass, as failure to break up cell clumps would lead to fairly inconsistent reduction. If the device cannot inactivate *M. smegmatis* at 3g or higher of *Mycobacterium spp.*, then we will have to conclude that it may be insufficient for the downstream applications where large biomass is needed.

Another limitation was the use of *M. smegmatis* as a model organism. We needed to demonstrate the ability of this technology to inactivate a near-neighbor BSL-1 organisms, before

moving it to the BSL-3 environment, for more rigorous testing on pathogenic *Mtb*. *M. smegmatis* is an environmental microorganism, which has been previously demonstrated to have resistance to UV-damage²⁸. Theoretically, UV + Riboflavin damage is more effective than UV alone, in that it causes irreversible DNA double-strand breaks, and this should not necessarily influence our results this way. Whether or not *Mtb* retains the same ability as *M. smegmatis* to resist UV damage, will also be covered in the following chapter.

We conclude that while high levels of inactivation are certainly possible, more work must be conducted to better characterize the damage that is occurring in *M. smegmatis*. We were able to demonstrate that damage is not a result of intrinsic genotypic resistance to this mechanism of inactivation. We also demonstrated that *M. smegmatis* is more resistant to this kind of damage than previously studied organisms²³, as well as *Mtb* in comparative studies. We will continue to interrogate these findings and their implications for the specific kind of damage occurring in treated cells.

Chapter 4 Introduction

UV-B and Riboflavin photochemistry is described through the occurrence of both Type I and Type II photosensitization⁴⁹. Both involve an electron transfer reaction from riboflavin in its triplet state, Type I conducting the transfer through substrate interaction, and Type II through transfer to oxygen^{23,49}. Type I photosensitization with riboflavin results in modification of the substrate, described in DNA most often as guanine base residues. This phenomenon has been described in bacterial, viral, and human DNA, in viable organisms and cell lines, as well as purified DNA preparations^{20,23,49}. Extensive 8-oxoguanosine formation is associated with failure in DNA replication, and cell death through apoptosis-like programmed death²³. Type II photosensitization results in singlet oxygen radicals, known to cause lesions in cellular DNA⁴⁹. Singlet oxygen species are associated as well with double and single strand breaks, and molecular shearing of DNA. Riboflavin photosensitization reactions have been demonstrated to cause shearing and breaks in viral, bacterial, and human DNA^{20,23,49} though it is uncertain if shearing is caused by oxygen radicals, programmed cell death, or both. Regardless, biomarkers of successful treatment can be found through primary detection of 8-oxoguanosine modifications and DNA shearing, as well as secondary confirmation of permeabilized membrane states in apoptotic cells.

Propidium Iodide (PI) staining has been well documented as an effective measure of viability through membrane permeability, a described biomarker of non-viability^{44,50}. PI enters inactivated cells, binds to DNA and RNA and fluoresces proportionally to the concentration of nucleic acids in each cell⁴⁴. This technique has been useful for identifying non-viable cells in

both eukaryotic, and prokaryotic culture⁵⁰, though it is commonly used in flow cytometric assays to measure apoptosis in eukaryotic cell lines⁴⁴. Apoptosis, which in this context may also be referred to as programmed cell death (PCD), is a well known response to stress by eukaryotic cells, however until recently its role in prokaryotes has been controversial^{51,52}. Highly conserved mechanisms of PCD have been described in bacterial cells⁵², and apoptosis-like cell death is a known biomarker of successful Mirasol pathogen reduction technology (MPRT) treatment²⁰. Regardless, properly inactivated cells uptake PI stain while living cells contain mechanisms to pump out PI⁵⁰. Due to its long-standing use in measuring both bacterial and eukaryotic cell viability, as well as simplicity of use, PI staining cheaply and robustly determines cell membrane permeability as a biomarker of photosensitizer specific damage.

The formation of 8-oxoguanosine base modifications is another well described biomarker of successful MPRT treatment^{20,23}. Colorimetric assays to measure concentrations of 8-oxoguanosine in DNA samples, have been developed using capture antibody ELISA⁵⁷⁻⁵⁹. Percentage capture of 8-oxoguanosine modifications by these assays is similar to that of HPLC, and the assay is cheaper and higher-throughput relative to traditionally described HPLC and LC-MS methods for 8-oxoguanosine detection⁵⁹.

Our previous study lead to the description significant reductions in culturable cells through dose response curves generated from the MPRT (reference previous chapter). Despite this reduction, complete inactivation of *M. smegmatis* was not accomplished, even at doses and cell concentrations significantly below those described in the literature²⁰. Cells re-cultured from surviving colonies, did not display different responses to MPRT treatment, suggesting that surviving cells did not contain a treatment-resistant genotype. Based on this result, we next explored markers of the effect of MPRT or photosensitization on treated cells. Our results here

show that we were unable to reliably detect any of the aforementioned markers of successful photosensitizer inactivation. In addition, PI staining showed no significant difference between riboflavin-positive, and riboflavin-negative MPRT-treated samples, while at the same time both were significantly less permeabilized than the controls.

From our results, we hypothesize that MPRT treatment to *M. smegmatis* culture generates UV-induced VBNCs. This hypothesis is supported by work from our collaborators demonstrating that *M. smegmatis* may not readily uptake riboflavin as effectively as its pathogenic partner, *Mtb* (Unpublished communication, Laboratory of DRS. Valerie Mizrahi and Digby Warner; University of Capetown). If so, this lack of ready uptake of the photosensitizing agent would prevent widespread Type I and Type II photosensitizer damage to the DNA of *M. smegmatis*, limiting damage to that caused by UV-B spectrum thymine-dimer formation. As previously mentioned, UV-treatment is well known to induce VBNC formation in bacteria^{38,39}, and *Mycobacterium spp.* have been shown to enter the dormant VBNC state^{40,41}. Since the VBNC state of bacteria is associated with maintained cell membrane structure and non-permeability, our flow assays which demonstrated a lack of membrane permeabilization in treated cells, also supports the idea of VBNC induction. Multiple DNA assays were performed to analyze DNA shearing, as well as 8-oxoguanine formation from photosensitizer damage, none of which determined that cellular DNA had interacted with UV-activated riboflavin. While support for this hypothesis is limited to the studies described in this thesis, it is undoubtedly a starting point for future and novel research on the induction of *M. smegmatis* VBNCs via UV light. Comparisons to *Mtb* also give insight into the reliability of *M. smegmatis* as a model organism for its pathogenic partner. This research demonstrated the need for future research into both riboflavin uptake of *Mycobacterium spp.*, and the stress-induced dormancy of VBNCs which

may lead to incorrect labeling of cells as non-viable. To elaborate in other words, we fear that lack of culturability may not be a strong enough indicator of cell non-viability, or death.

Materials and Methods

DNA Isolation and Purification

Bacterial pellets were suspended in 10 ml of TE Buffer each and transferred to Teflon Oakridge tubes. Ten ml of 2:1 chloroform-methanol was added to each pellet, and samples incubated at room temperature for 30 minutes, and centrifuged at 2500 x g for 20 minutes at 4°C. Aqueous and organic layers were decanted, and pellets were left to air dry overnight. Cells were resuspended in 20 ml TE buffer, and vortexed to break up clumps. Two ml of 1M Tris-HCl, pH = 9.0 was added to each tube, and placed on a 55°C water bath for 30 minutes, followed vortexing again to break up clumps. Lysozyme was added to each tube at 300µg/ml and incubated at 37°C for 16 hours. Two ml of 10% SDS, 200µl of Proteinase K (10mg/ml) and 100µl RNase (1mg/ml) was added to each tube, placed on a 55° water bath for 3 hours, with mixing by inverting every 30 minutes. Twenty ml of 25:24:1 phenol-chloroform-isoamyl alcohol and rocked at room temperature for 30 minutes, followed by centrifugation at 12,000 x g for 30 minutes at 4°C. The upper aqueous layer of each tube was transferred to 50ml Teflon Oakridge tubes, with 20ml 24:1 chloroform-isoamyl alcohol added to each. Tubes were rocked again for 10 minutes at room temperature, and centrifuged at 12,000 x g for 30 minutes at 4°C. Again, the upper aqueous layers of each tube were transferred to 50ml Teflon Oakridge tubes, filled with 2ml 3M sodium acetate, pH=5.2 and 20ml isopropanol. Tubes were inverted 2-3 times each, and placed at 4°C for 16 hours. Concentrations were then centrifuged at 12,000 x g for 30 minutes at 4°C, the supernatant was decanted, 30ml of -20° ethanol was added to each, and then centrifuged again under the same conditions. Ethanol was decanted, and pellets were air-dried and

resuspended in 5ml TE buffer. Two μ l aliquots were analyzed on NanoDrop2000 against TE buffer blanks to measure DNA concentrations and purity.

Sau3A and EcoR1 Digestion Assays

For Sau3A restriction enzyme, all reagents were acquired from New England Biolabs restriction enzyme kit catalog # R0169S. The reaction was performed with the addition, in order, of 10 units Sau3A restriction enzyme, 1 μ g each sample of DNA, 5 μ l of 10X NEBuffer, brought to a volume of 50 μ l with DEPC-treated water. The reaction was performed at 37°C for 60 minutes, and stopped using 10 μ l NEB stop buffer. For EcoR1 restriction enzyme, all reagents were acquired from New England Biolabs restriction enzyme kit catalog #R3101S. The reaction was initiated with the addition, in order, of 1 μ l EcoR1 restriction enzyme, 1 μ g each sample of DNA, 5 μ l of 10X NEBuffer, brought to a volume of 50 μ l with DEPC-treated water and was performed by incubating samples at 37°C for 15 minutes, and stopped by adding 10 μ l of NEB stop buffer/6X loading dye.

DNA Gel Electrophoresis

All gels were made with 1.0% pure Agarose in 1X TAE buffer and 20 μ l SYBR safe DNA gel stain (Thermo Scientific). DNA concentrations were standardized to 500 ng in 20 μ l per well. Each concentration was added to a well in the DNA gel, with the addition of 5 μ l 6x loading buffer, except for EcoR1 treated DNA which had 6x loading buffer in its stop solution. The gels were run at 95 volts for 90 minutes.

PI Flow Cytometric Assay

Two *M. smegmatis* pellets were treated in MPRT bags at 8,640 J containing 20-30g pellets, 270 ml of GAS media, and 30 ml of 500 μ M riboflavin for a final concentration of 50 μ M. Two pellets were treated under the same conditions, but riboflavin was substituted with an

additional 30 ml of GAS media, so that there was equal volume but no photosensitizing agent. One ml was taken from each bag pre-treatment to determine CFU/ml, and 10 ml samples were aliquoted from each bag post-treatment. A 24.71 g pellet of *M. smegmatis* was suspended in 142 ml of GAS media, and 6 mg of moxifloxacin fluoroquinolone was added, for a final concentration of 42 µg/ml, the MIC₉₉ of the antibiotic in *M. smegmatis* as determined by Malik M et al⁶¹. One ml was taken before addition of moxifloxacin, then diluted and plated for CFU counts. This sample, to serve as an inactivated control based on similar mechanism of action, was incubated at 37°C for 16 hours, where again one ml was taken from each bag pre-treatment to determine CFU/ml, and 10 ml were taken from each bag post-treatment for potential downstream applications, namely flow cytometry. Samples were further diluted 1:100 in 10 ml PBS, in 15 ml conical tubes. Tubes were spun at 2,500 x g for 10 minutes at room temperature, supernatant was removed, and pellets were resuspended in 10 ml PBS. 100 µl of RNase was added to each conical, and placed in a 55°C water bath for 30 minutes. Tubes were centrifuged again at 2,500 x g for 10 minutes at room temperature, supernatant was removed, and pellets were resuspended in 10 ml PBS. A 3 ml aliquot was transferred from each sample to round-bottom polystyrene FACS tubes in triplicate, and concentrated with 1 µg/ml PI stain. An unstained, untreated reference group of cells was transferred to one tube, as well as a live-dead control consisting of 5 ml untreated cells, and 5 ml moxifloxacin-treated cells. The live-dead control was also concentrated with 1 µg/ml PI stain. Samples were read using a 4-laser aurora flow cytometer, analyzing for red fluorescence (>600 nm). Flow cytometry gates were determined based on live-dead controls (Appendix B).

8-oxoguanosine Damage Quantification Assay

The EpiQuik™ 8-OHdG DNA Damage Quantification Direct Kit (EpiGenTek catalog #P-6003) was used to measure 8-oxoguanosine and performed following manufacturers protocol. The positive control standard curve was generated, in duplicate, with concentrations of 5, 10, 20, 50, 100, and 200 pg of 8-oxoguanosine. Negative controls contained reagent buffers only, and a non-treated 300 ng *M. smegmatis* DNA controls were treated in duplicate. Three-hundred ng DNA from 360J, 720J, 2880J, 5760J, 8640J + riboflavin, and 8640J – riboflavin, were added in duplicate to samples wells. Samples sat in binding solution for an hour and half, before being washed three times with wash buffer solution. Capture antibody was added, incubated at room temperature for one hour, and wells were washed three times. Detection antibody was added, incubated at room temperature for one half hour, and wells were washed four times. Enhancing solution was added, incubated at room temperature for one half hour, and wells were washed five times. One hundred µl of developing solution was added to each well for 5 minutes and stopped using stop solution. Plates were read on a plate reader at 450 nm for colorimetric detection of 8-oxoguanosine against the standard curve.

Results

Quality of DNA

Standard gel electrophoresis performed on crude DNA extracts did not demonstrate strand shearing patterns characteristic of MPRT photochemistry (Figure 9A). We did not observe damage to DNA that had been described in the literature, nor could we find differences in appearance between the control and treated nucleotides. DNA treated with restriction enzyme Sau3A displayed bands in the expected 200-2000 bp range, as had been previously described in the literature⁶⁰ (Figure 9B). Bands did not appear below the lower end of the range, and MPRT treated DNA was not noticeably different in appearance on the gel, compared to the untreated

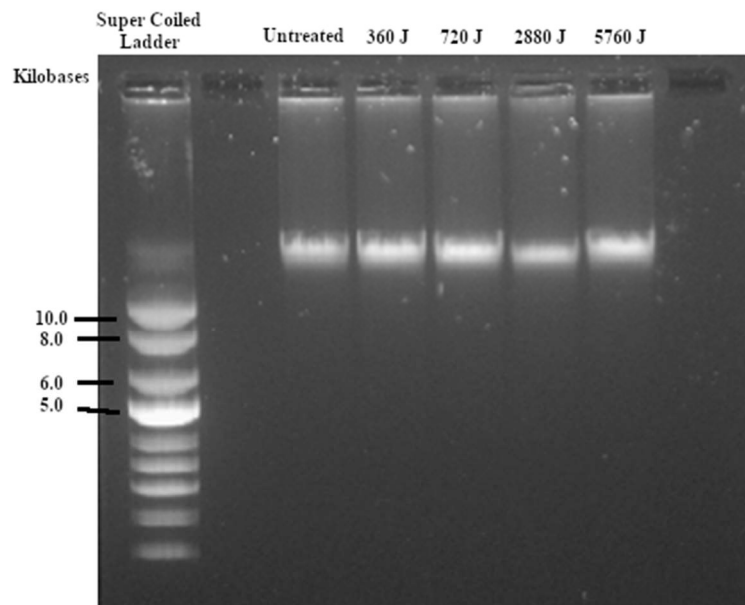
control and UV-RB treatment. EcoR1 restriction enzyme-treated DNA from our dose response curve generated similar results, as photosensitizer-characteristic shearing did not appear to take place (Figure 9C). EcoR1 treated bands did appear to get lighter in pixels as Joule dose to DNA increased, but this did not indicate any significant patterns when contextualized with UV treatment or control DNA.

Flow Cytometry

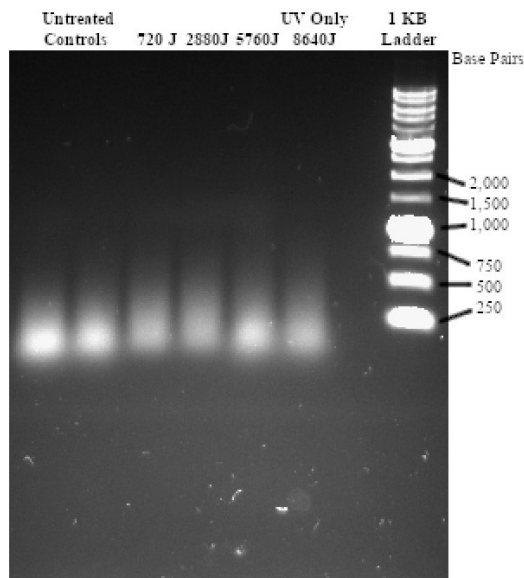
PI did not enter MPRT treated cells and bind to cellular DNA as readily as the moxifloxacin control group (Figure 10). Permeabilized cells, as indicated by PI fluorescence and based on live-dead P4 parent gating, made up on average less than half of cells in each MPRT treatment group, despite 6-7 log reductions in culturable cells. Furthermore, there was not a significant difference in non-viable cells between riboflavin + and riboflavin – UV treated cells. While moxifloxacin MIC₉₉ and MPRT treatment groups retain similar reductions in culturable cells, there were clear differences in proportion of non-viable cells as defined by loss of membrane integrity. Cell concentrations were standardized based on final CFU/ml after treatment.

8-oxoguanosine Detection Assays

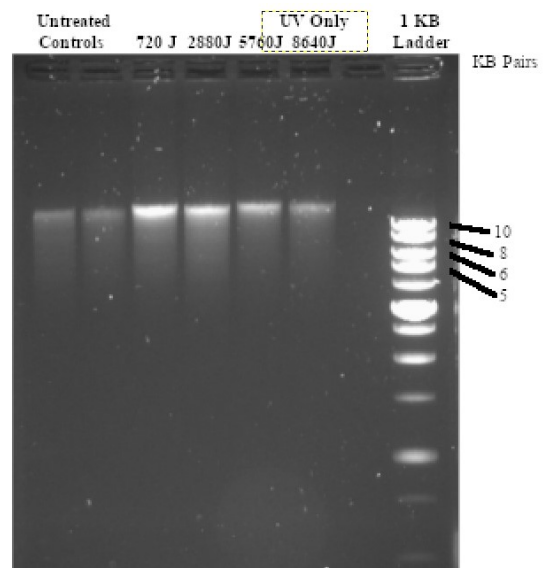
No discernable pattern of increased 8-oxoguanoside detection was observed in increasing treatment groups (Table 3). The literature describes basal levels of 8-oxoguanosine to be generally lower than 0.01% of total nucleotide content⁵⁹, as indicated on the standard curve by a blue transparent box (Figure 11). None of the treated samples exceed this 30 pg predicted range. Furthermore, most treatment 8-OHdG levels do not exceed the UV – riboflavin control, and hardly exceed the non-treated DNA control (Table 3).



A



B



C

Figure 9 (above). 1.0% agarose gels run on DNA from MPRT-treated cells. (A) Shows crude DNA run for 95 minutes at 95 volts, increasing Joule doses compared to a non-treated control. (B) Sau3A restriction enzyme product from the same DNA samples was run on a gel under similar conditions. (C) Similarly, this was performed with EcoR1 restriction enzyme.

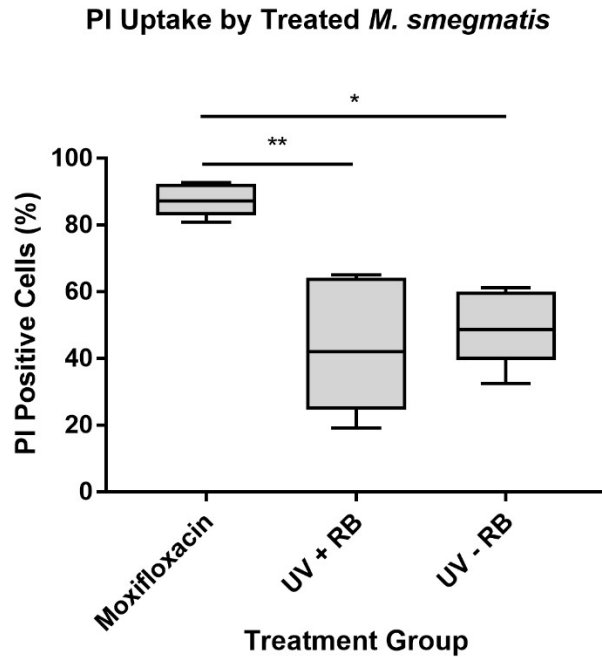


Figure 10 (above). PI uptake measured proportionally by flow cytometry as described in the methods. Moxifloxacin inactivated cells uptook PI at a mean of 87.37%, with a standard error of 2.13. These numbers were 43.19% +/- 8.46 and 49.66% +/- 5.10 for UV + RB and UV – RB treatment groups respectively. Significance determined by Kruskal-Wallis nonparametric analysis of variance. * indicates $p < 0.05$, ** indicates $p < 0.005$

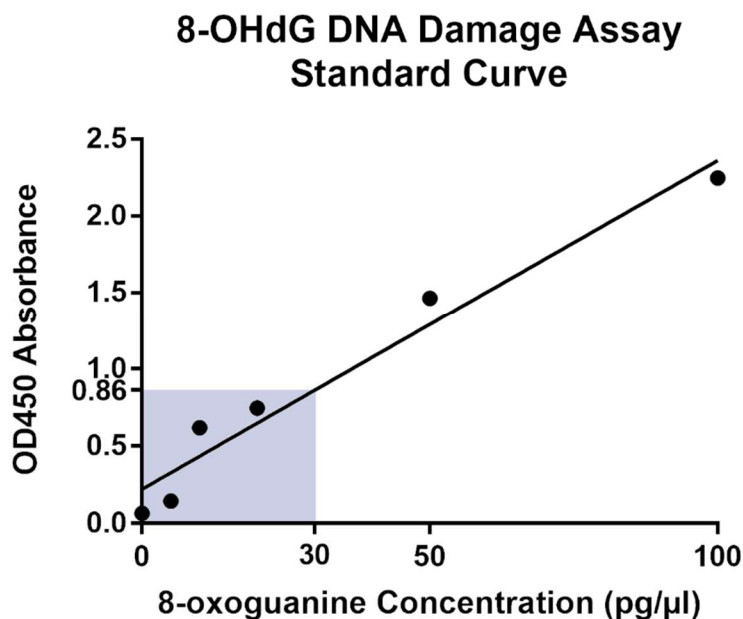


Figure 11 Standard Curve 8-OHdG Assay and Table 3 8-OHdG Replicates (above). Analysis of 8-oxoguanosine formation in treated DNA. The standard curve was generated from OD450 absorbance of 0, 5, 10, 20, 50 and 100 pg/μl 8-OHdG positive control. The linear model can be described as $y=0.0214(x) + 0.2214$, with an R^2 value = 0.96.

Table 3 (below). From the curve, approximate 8-OHdG quantity in ng was calculated using the equation: $8\text{-OHdG (\%)} = (\text{Sample OD450} - \text{Negative Control OD450}) / \text{Standard Curve Slope}$.

Treatment	Riboflavin	8-OHdG (ng) Replicate 1	8-OHdG (ng) Replicate 2
0 J	negative	0.025	0.475
360 J	positive	4.575	12.575
720 J	positive	0.175	-0.075
2880 J	positive	2.975	3.225
5760 J	positive	0.275	0.375
8640 J	positive	0.325	0.975
8640 J	negative	0.575	0.775

Chapter 4 Conclusions and Discussion

We have demonstrated that *M. smegmatis* maintains a high level of resistance to MPRT treatment, beyond just capturability as described in Chapter 3, but also in traditional biomarkers of non-viability that do not translate in the *M. smegmatis* model, even after significant reductions in culturable cells is achieved. *M. smegmatis* DNA, after high doses of treatment from MPRT,

does not undergo any shearing or damage, even when treated with restriction enzyme to reduce fragment size and better observe shearing, we see no noticeable difference between the treatment groups and the control. We also do not see differences between riboflavin + and riboflavin – DNA, as has been previously observed in *E. coli* cells undergoing the same treatment at similar concentrations²⁰. Flow cytometric assays indicate that there is nearly no permeability of the cell membranes of treated cells. Moxifloxacin was used as a control, because of its effective inactivation of *M. smegmatis*. In addition, it has a similar mechanism of inducing PCD, but instead of generating 8-oxoguanosine base modifications like MPRT, it instead inhibits DNA gyrase activity to prevent replication and force PCD⁶². While moxifloxacin treatment lead to nearly 90% membrane permeability in treated *M. smegmatis* cells, MPRT treatment was significantly lower as measured by the 4-laser Aurora flow cytometer. Additionally, we saw no significant difference in permeabilized cells post-treatment between cells treated with UV + riboflavin, and UV – riboflavin. This indicates that the induction into the PCD state is not occurring uniquely in either sample. There was not full uptake in moxifloxacin controls either, which can be explained by a few possibilities. Since PI was standardized to cell concentration, this does not hurt the integrity of the work. Likely, there may be some VBNC formation in the moxifloxacin treated cells. Another possibility is that the concentration of PI was too low in samples to completely stain dead controls. These are both things that could be refined in further protocols, however due to standardization, the purpose and interpretation of the data remains the same.

8-oxoguanosine evidence was particularly compelling, because formation of the mutated guanosine motif is the primary biomarker of successful MPRT treatment. The lack of significant differences between UV + RB treated, UV – RB treated, and the control DNA, told a compelling

story regarding riboflavin uptake and the lack of differences in treatment. It was not demonstrated that 8-oxoguanosine formation was occurring any more readily in treated samples, compared to the standard or DNA control.

While *M. smegmatis* has long been described as capable of VBNC state dormancy, we have not been able to find previous work in the literature that fully describes the process of UV-induced VBNCs in *M. smegmatis*. This work could very easily translate to preliminary evidence of such a phenomenon. Another fascinating aspect of the research in this chapter is the future work it may spark in describing exogenous uptake of riboflavin, and how that may have implications for successful MPRT treatment. This extends beyond just large-scale culture, as MPRT is commonly used in hospitals to inactivate pathogens in plasma products. While *M. smegmatis* is not a human pathogen, the possibility of other organisms which display similar characteristics of resistance should not be ignored. If it is in fact the case that *M. smegmatis* is refractory to uptake of exogenous riboflavin, and also the case that it enters a hardy VBNC dormancy state from UV-induction, then it is also possible that this mechanism of resistance is not unique. VBNC dormancy is associated with many other increases in anti-microbial resistance, and its potential to challenge effective inactivation of some opportunistic pathogens should not be ignored.

CHAPTER 5: CONCLUDING REMARKS AND FUTURE DIRECTIONS

Inactivation techniques, despite their previously demonstrated successes or long-standing reputations, should always continue to be interrogated and improved upon so that we can better understand the negative attributes associated with each. Inactivation of pathogens from large-scale culture plays a crucial role in research, food safety, and transfusion of plasma products. However, the consequences of incomplete inactivation can be devastating, and improving our knowledge of subjects relating to inactivation helps us better understand our protocols, model organisms, and safe manipulation of pathogens to prevent laboratory acquired exposure or infection.

This work demonstrated the potential for UV-induced VBNCs in *M. smegmatis* culture when treated with MPRT to inactivate microbial pellets from large-scale culture. As discussed previously, *M. smegmatis* is commonly used as a non-pathogenic model organism from which studies in its pathogenic neighbor, *Mtb*, are often extrapolated. From this basis, we hypothesized that our studies performed in *M. smegmatis* would translate to similar success or failure in *Mtb*. Given that MPRT was incapable of completely inactivating *M. smegmatis* – even at high doses with CFU below 10^7 – we predicted that *Mtb* would be similarly resistant. We conducted studies in *Mtb* and found that it was completely inactivated by CFU, Alamar Blue, and Mycobacterial Growth Indicator Tube (MGIT), with one exception in a single MGIT replicate at the 8640J dose (Supplementary Figures 1 and 2). Because of its unusually quick growth on 7H11, we suspect some kind of contamination, despite acid fast bacillus positive staining. Interestingly, *Mtb* may uptake more riboflavin than its model organism *M. smegmatis*. The hypothesized reluctance of *M. smegmatis* to uptake riboflavin as actively as its pathogenic partner, *Mtb*, should be further

studied to better understand the relationship between the two organisms. Studies focusing on the genomic, proteomic and metabolomic differences in riboflavin synthesis in *Mycobacteria spp.* are abundant. More neglected is work demonstrating the mechanisms by which riboflavin enters cells from exogenous sources. Many prokaryotes have developed methods for endogenous synthesis of riboflavin, a necessary cofactor for various metabolic functions⁶⁸. For this reason, perhaps, dogma has limited the studies of riboflavin uptake by cells. While it is true that many bacteria have not developed methods to uptake riboflavin because of their established methods of endogenous synthesis⁶⁸, it is clear through the success of MPRT in a variety of bacteria and viruses that riboflavin is taken in by cells. *E. coli*, for example, is highly successfully treated with MPRT²⁰, while endogenous riboflavin synthesis pathways remain conserved⁶⁸. The differences in culturability between *Mtb* cells, and *M. smegmatis* cells following riboflavin photochemical treatment, does not in and of itself prove the differences in riboflavin uptake hypothesized. However, the ability to completely render *Mtb* non-culturable does imply differences in response to MPRT treatment. This has implications not only for MPRT as a mechanism of inactivating organisms from large-scale culture, but also future work in the field that may better characterize *M. smegmatis*, and when exactly it is an appropriate model of *Mtb*.

More work too can, and should focus on UV induction of VBNC-state dormancy in both *M. smegmatis* and potentially *Mtb*. While our data supports such a hypothesis, our studies are limited by their scope. More work could be done to establish other biomarkers of VBNC formation in *Mycobacterium spp.* Even further, studies can be conducted to measure the odds of reactivation. For example, if more robust genetic biomarkers of VBNC dormancy are established in *M. smegmatis* models, one could determine if colonies isolated on post-MPRT-treatment culture plates, are incidental, or the result of re-activated from previously non-culturable

organisms. There is mounting evidence that VBNCs pose a risk, not only because of their increased resistance to typical methods of inactivation, but also their ability for reactivation. If such mechanisms are conserved across *Mycobacterium spp.*, as we seem to have observed in *M. smegmatis*, then what implications does this have for *Mtb* that is thought to have been inactivated because it is no longer culturable. Furthermore, what are the odds of it, or other pathogens, reactivating after being presumed to be dead?

Future work should also focus on *Mtb* inactivation. This includes the 8-oxoguanosine experiments, and flow cytometry assays performed on *M. smegmatis*. Additionally, since complete inactivation is possible with *Mtb*, metabolic, enzymatic and structural assays should be performed to better characterize actual damage. Some of these assays may include KatG assays, LDH assays, and broad genomic and proteomic analysis of treated *Mtb* compared to wildtype controls. Controls should also consist of gamma-irradiated cells, as the current gold-standard for inactivation. These will give insight into the type of damage done on completely inactivated cells, which we could not achieve with *M. smegmatis*. Additionally, it will be worthwhile to conduct similar work in other organisms, particularly select agents. Anecdotally, in preliminary work, BSL-2 variants of *Yersinia pestis* were completely inactivated at low doses, however these experiments can be better developed for future studies (data not shown).

The establishment of a D₁₀ model for Cs-137 inactivation was an exciting byproduct of this thesis. The utility of this dose-response curve, will be apparent for future calibration of our source. Further work must be done down the line to establish differences in D₁₀ values as the Cs-137 source continues to decay. A biological method for calibration is an exciting stepping stone for both reliability of the source, and comparative studies to analyze how well Cs-137 renders *Mtb* non-culturable and non-viable. To our knowledge, this is the first D₁₀ curve that has been

established for Cs-137 source inactivation of *Mtb*, and it will be useful for further studies looking at the effectivity of irradiation over time. Balancing that information with changes in cost, safety, or operation, are also crucial.

While the work in this thesis has closed gaps in knowledge, it has also drawn new questions about the way we model pathogens, and hold accountable our methods of inactivation. The differences between *Mtb* and *M. smegmatis* are almost always analyzed through the lens of genetic similarity, and because of their closely related nature, *M. smegmatis* has long been assumed to be an adequate near-neighbor model of *Mtb*. What has more seldomly been acknowledged is the differences between organisms that must be interrogated before using one to model the other. *M. smegmatis*, after all, is an environmental organism, that survives well outside the human body, and replicates at nearly six times the rate of *Mtb*. Despite its widespread use as a model for disease, it will be worthwhile to better understand the limitations of *M. smegmatis* in such a context. Ultimately, we have come to better understand methods of inactivation, *M. smegmatis* as a near-neighbor model for *Mtb*, and a potentially novel understanding of UV-induced VBNC dormancy in mycobacteria. It is our hope that future work can piggyback off of these concepts, to better understand *M. smegmatis* as a model organism, and MPRT as a method for inactivating Mycobacteria and other *Actinomyces*. Additionally, the success seen in *Mtb* may indicate potential for the device to replace traditional methods of inactivation. If it is further demonstrated to inactivate *Mtb* reliably, and reproducibly, it may serve some utility for laboratory applications related to complete inactivation of large cell pellets. This would be exciting, because of the relatively low cost, and high level of safety when working with the device. Regardless, inactivation via MPRT has continuing utility in hospital settings, as well as vaccine development for susceptible organisms.

REFERENCES

1. Van Soolingen et al., Practical biosafety in the tuberculosis laboratory: containment at the source is what truly counts. *Int J Tuberc Lung Dis* 18(8):885–889 (2014).
2. Wilson DE, Memarzadeh F, National Institutes of Health Biosafety Level 3 Laboratory Certification Requirements. National Institute of Health (2006).
3. Merler S, Ajelli M, Fumanelli L, et al. Containing the accidental laboratory escape of potential pandemic influenza viruses. *BMC Med* 11, 252 (2013).
4. Lipsitch M, Bloom BR. Rethinking biosafety in research on potential pandemic pathogens. *mBio* 3(5):e00360-12 (2012).
5. Ssengooba et al., Feasibility of establishing a biosafety level 3 tuberculosis culture laboratory of acceptable quality standards in a resource-limited setting: an experience from Uganda. *Health Research Policy and Systems* 13, Article number: 4 (2015)
6. Parsons LM et al., Laboratory Diagnosis of Tuberculosis in Resource-Poor Countries: Challenges and Opportunities. *Clinical Microbiology Reviews* Apr. 2011, p. 314–350
7. Homer LC et al., Guidelines for Biosafety Training Programs for Workers Assigned to BSL-3 Research Laboratories. *Biosecurity and Bioterrorism: Biodefense Strategy, Practice, and Science* Vol. 11, No. 1 (2013).
8. Coppola M, Stedman TT, Overheim K, Gibbons J, Rashid S., Public Health Emergency Preparedness and Response Applied Research. American Type Culture Collection (2019).

9. Garcia MM et al., Evaluation of gamma radiation levels for reducing pathogenic bacteria and fungi in animal sewage and laboratory effluents. *Can J Vet Res.* 1987 Jul;51(3): 285-289.
10. Kubín M, Sedlácková J, Vacek K, Ionizing radiation in the disinfection of water contaminated with potentially pathogenic mycobacteria. *J Hyg Epidemiol Microbiol Immunol.* 1982;26(1):31-6.
11. Marcinko R, “Calibration of an Irradiation Facility,” thesis, Colorado State University, Fort Collins, CO (2017).
12. Sudprasert W, Navasumrit P, Ruchirawat M, Effects of low-dose gamma radiation on DNA damage, chromosomal aberration and expression of repair genes in human blood cells. *International Journal of Hygiene and Environmental Health Volume 209, Issue 6, 15 November 2006, Pages 503-511*
13. Global tuberculosis report 2019. Geneva: World Health Organization; 2019. Licence: CC BY-NC-SA 3.0 IGO
14. Lasch P et al., Identification of Highly Pathogenic Microorganisms by Matrix-Assisted Laser Desorption Ionization–Time of Flight Mass Spectrometry: Results of an Interlaboratory Ring Trial. *Journal of Clinical Microbiology* 53 (8) 2632-2640 (2015).
15. Hayhurst A et al., Isolation and expression of recombinant antibody fragments to the biological warfare pathogen *Brucella melitensis*. *Journal of Immunological Methods* Volume 276, Issues 1–2, 185-196 (2003).

16. Magnani DM, Harms JS, Durward MA, Splitter GA, Nondividing but Metabolically Active Gamma-Irradiated *Brucella melitensis* Is Protective against Virulent *B. melitensis* Challenge in Mice. *Infection and Immunity* 77 (11) 5181-5189 (2009).
17. Alsharifi, M; Müllbacher, A, The [gamma]-irradiated influenza vaccine and the prospect of producing safe vaccines in general. *Immunology and Cell Biology* Vol. 88, Iss. 2, (2010).
18. Oliveira SC, Zhu Y, and Splitter GA, Recombinant L7/L12 ribosomal protein and gamma-irradiated *Brucella abortus* induce a T-helper 1 subset response from murine CD4⁺ T cells. *Immunology* 83(4): 659–664 (1994).
19. Brandl A, Bell J, Dosimetric Evaluation of a CS-137 Irradiator Located in Room 004 of the Molecular and Radiological Biosciences Building Utilizing Various Radiation Measurement Methods. Colorado State University Department of Environmental and Radiological Health Sciences (2016).
20. Goodrich R, Keil SD. Induction of Maintenance of Nucleic Acid Damage in Pathogens using Riboflavin and Light. United States Patent US 7,985,588 B2. 2011.
21. Rastogi R et al. Molecular Mechanisms of Ultraviolet Radiation-Induced DNA Damage and Repair. *Journal of Nucleic Acids* 2010; 2010:1-32.
22. Mirshafiee H., Sharifi, Z., Hosseini, S. M., Yari, F., Nikbakht, H., & Latifi, H. The effects of ultraviolet light and riboflavin on inactivation of viruses and the quality of platelet concentrations at laboratory scale. *Avicenna J Med Biotech* 2015, 7(2):57-63.
23. Kumar V, Lockerbie O, Keil SD, Ruane PH, Platz MS, Martin CB, et al. Riboflavin and UV-light based pathogen reduction: extent and consequence of DNA damage at the molecular level. *Photochem Photobiol* 2004; 80: 15– 21

24. Rampersad SN, Multiple Applications of Alamar Blue as an Indicator of Metabolic Function and Cellular Health in Cell Viability Bioassays. *Sensors (Basel)* 2012; 12(9): 12347–12360.
25. Voytik-Harbin S.L., Brightman A.O., Waisner B., Lamar C.H., Badylak S.F. Application and evaluation of the Alamar Blue assay for cell growth and survival of fibroblasts. *In Vitro Cell Dev. Biol. Anim.* 1998;34:239–246.
26. Bwanga F., Joloba M.L., Haile M., Hoffner S. Evaluation of seven tests for the rapid detection of multidrug-resistant tuberculosis in Uganda. *Int. J. Tuberc. Lung Dis.* 2010;14:890–895.
27. Kuratomi K, Kobayashi Y. Studies on the Interaction between Flavins and DNA. *Biochemica et Biophysica acta* 1977; 476: 207-217.
28. Hu JJ et al. The Effect of Hydrogen Peroxide on DNA Repair Activities. *Mutation Research* 1995; 336(2): 193-201.
29. Mirshafiee H, Sharifi Z, Hosseini SM, et al. The Effects of Ultraviolet Light and Riboflavin on Inactivation of Viruses and the Quality of Platelet Concentrates at Laboratory Scale. *Avicenna Journal of Medical Biotechnology*. 2015 Apr-Jun;7(2):57-63.
30. Singh AK, Reyrat JM. Laboratory maintenance of *Mycobacterium smegmatis*. *Curr Protoc Microbiol.* 2009;Chapter 10:Unit10C.1.
31. Yamada H et al. Can *M. smegmatis* be used as a real alternative for *M. tuberculosis*? *European Respiratory Journal* 2016 48.
32. Gupta R et al. *Mycobacteria* Exploit Three Genetically Distinct DNA Double Strand Break Repair Pathways. *Molecular Microbiology* 2011; 79(2): 316-330.

33. Li XZ, Zhang L, Nikaido H. Efflux Pump-Mediated Intrinsic Drug Resistance in *Mycobacterium smegmatis*. *Antimicrobial Agents and Chemotherapy* Jun 2004, 48 (7) 2415-2423.
34. Flores AR, Parsons LM, Pavelka, Jr MS. Genetic analysis of the β -lactamases of *Mycobacterium tuberculosis* and *Mycobacterium smegmatis* and susceptibility to β -lactam. *Microbiology* (2005), 151, 521–532.
35. Szeto W, Yam WC, Huang H, Leung DY. The efficacy of vacuum-ultraviolet light disinfection of some common environmental pathogens. *BMC Infect Dis*. 2020;20(1):127. Published 2020 Feb 11. doi:10.1186/s12879-020-4847-9
36. CDC Report on the Potential Exposure to Anthrax (CDC, 2014).
37. Trevan T. Biological Research: Rethink Biosafety. *Nature* Nov. 2015, 7577(527).
38. Li, Laam et al. “The importance of the viable but non-culturable state in human bacterial pathogens.” *Frontiers in microbiology* vol. 5 258. 2 Jun. 2014.
39. Robben, C., Fister, S., Witte, A.K. et al. Induction of the viable but non-culturable state in bacterial pathogens by household cleaners and inorganic salts. *Sci Rep* 8, 15132 (2018).
40. Anuchin A. M., Mulyukin A. L., Suzina N. E., Duda V. I., El-Registan G. I., Kaprelyants A. S. (2009). Dormant forms of *Mycobacterium smegmatis* with distinct morphology. *Microbiology* 155, 1071–1079
41. Kuznetsov B. A., Davydova M. E., Shleeva M. O., Shleev S. V., Kaprelyants A. S., Yaropolov A. I. (2004). Electrochemical investigation of the dynamics of *Mycobacterium smegmatis* cells' transformation to dormant, nonculturable form. *Bioelectrochemistry* 64, 125–131

42. Gourmelon M., Cillard J., Pommepuy M. (1994). Visible light damage to *Escherichia coli* in seawater: oxidative stress hypothesis. *J. Appl. Bacteriol.* 77, 105–112.
43. Oliver J. D. (2010). Recent findings on the viable but nonculturable state in pathogenic bacteria. *FEMS Microbiol. Rev.* 34, 415–425
44. Riccardi, C., Nicoletti, I. Analysis of apoptosis by propidium iodide staining and flow cytometry. *Nat Protoc* 1, 1458–1461 (2006).
45. Cebrián, Guillermo et al. “Physiology of the Inactivation of Vegetative Bacteria by Thermal Treatments: Mode of Action, Influence of Environmental Factors and Inactivation Kinetics.” *Foods* vol. 6,12 107. 30 Nov. 2017.
46. Van Asselt ED., Zwietering MH. “A systematic approach to determine global thermal inactivation parameters for various food pathogens.” *International Journal of Food Microbiology* 107(1) 73-82 (2006).
47. Spinks AT et al. “Thermal inactivation of water-borne pathogenic and indicator bacteria at sub-boiling temperatures.” *Water Research* 40(6) 1326-1332 (2006).
48. Sagripanti, Jose-Luis et al. “Microbial inactivation for safe and rapid diagnostics of infectious samples.” *Applied and environmental microbiology* vol. 77,20 (2011).
49. Ito K., Inoue K., Kawanishi S. “8-Hydroxydeoxyguanosine Formation at the 5′ Site of 5′-GG-3′ Sequences in Double-stranded DNA by UV Radiation with Riboflavin.” *Journal of Biological Chemistry* 268(18) 13221-13227 (1993).
50. Davies D. “Flow cytometric analysis of cell cycle with propidium iodide DNA staining.” *Abcam*.
51. Hochman A. “Programmed cell death in prokaryotes.” *Crit Rev Microbiol.* 1997;23(3):207-214.

52. Bayles, Kenneth W. "Bacterial programmed cell death: making sense of a paradox." *Nature reviews. Microbiology* vol. 12,1 (2014): 63-9.
53. Rock G. "A comparison of methods of pathogen inactivation of FFP." *The International Journal of Transfusion Medicine* 100(2) 169-178 (2011).
54. Lin A et al. "Effects of bacterial inactivation methods on downstream proteomic analysis." *Journal of Microbiological Methods* 112 3-10 (2015).
55. Mitra G., Wong M. "Use of Lipid Solvents for Viral Inactivation in Factor VIII Concentrates." *Biotechnology and Bioengineering*, Vol. XXVIII, Pp. 297-300 (1986).
56. Feinstone SM et al. "Inactivation of Hepatitis B Virus and Non-A, Non-B Hepatitis by Chloroform." *Infection and Immunity* 41(2) 816-821 Aug. 1983.
57. Kim SY et. al. "Attractive male sticklebacks carry more oxidative DNA damage in the soma and germline." *J Evol Biol*. 2019.
58. Yuan L et. al. "Aloe polysaccharide protects skin cells from UVB irradiation through Keap1/Nrf2/ARE signal pathway." *J Dermatolog Treat*. :1-9 (2019).
59. EpiGentek. (2014). EpiQuik™ 8-OHdG DNA Damage Quantification Direct Kit (Colorimetric). Retrieved from <https://www.epigentek.com/catalog/epiquik-ohdg-dna-damage-quantification-direct-kit-colorimetric-p-2930.html>.
60. Spratt JM., Britton WJ., Triccas JA. "Identification of strong promoter elements of *Mycobacterium smegmatis* and their utility for foreign gene expression in mycobacteria." *FEMS Microbiology Letters* 224(1) 139-142 (2003).

61. Guilhot C., Gicquel B., Davies J., Martin C. "Isolation and Analysis of IS6120, a new insertion sequence from *Mycobacterium smegmatis*." *Mol Microbiol* **6**:107-113 (1992).
62. Malik M., et al. "Lethality of Quinolones against *Mycobacterium smegmatis* in the presence or absence of Chloramphenicol." *Antimicrobial Agents and Chemotherapy* **49**(5) 2008-2014 (2005).
63. Cote, C.K., et al. "A Standard Method to Inactivate Bacillus anthracis Spores to Sterility Using gamma-Irradiation." *Appl Environ Microbiol*, 2018. **84**(12): p. e00106-18.
64. Bodgi, L., et al. "Mathematical models of radiation action on living cells: From the target theory to the modern approaches." A historical and critical review. *Journal of Theoretical Biology*, 2016. **394**:p. 93-101.
65. Russell AD. The destruction of bacterial spores. Academic Press, Cambridge, MA (1982).
66. Dauphin LA, Newton BR, Rasmussen MV, Meyer RF, Bowen MD. Gamma irradiation can be used to inactivate Bacillus anthracis spores without compromising the sensitivity of diagnostic assays. *Appl Environ Microbiol* **74**:4427–4433 (2008).
67. Parisi AN, Antoine AD. "Characterization of Bacillus pumilus E601 spores after single sublethal gamma irradiation treatments." *Appl Microbiol* **29**:34–39 (1975).
68. Long Q, Lei J, Wang H, Xie J. "Riboflavin Biosynthetic and Regulatory Factors as Potential Novel Anti-Infective Drug Targets. *Chem Biol Drug Des*; **75**:339-347. (2010)."

69. Saviola B. Mycobacterium tuberculosis Adaptation to Survival in a Human Host, *Tuberculosis - Current Issues in Diagnosis and Management*, Bassam H. Mahboub and Mayank G. Vats, IntechOpen, (2013).
70. Shiloh, MU, Patricia ADC. "To catch a killer. What can mycobacterial models teach us about Mycobacterium tuberculosis pathogenesis?." *Current opinion in microbiology* vol. 13,1 (2010): 86-92.
71. Cronk TM. "Work Vows DoD's Live Anthrax Incident 'Will Never Happen Again.'" *U.S. Department of Defense*. 2015.
72. deAlmeida CE, Ochoa R, Lima MC, et al. A feasibility study of Fricke dosimetry as an absorbed dose to water standard for ¹⁹²Ir HDR sources. *PLoS One*. 2014;9(12):e115155. 2014.
73. Butson M J, Yu P K N, Cheung T and Metcalfe. Radiochromic film for medical radiation dosimetry Mater. Sci. Eng. R 41 61-120. 2003.
74. Cameron J. Radiation Dosimetry. *Environmental Health Perspectives* Vol.91, pp. 45-48, 1991.

APPENDIX A

Method 1. Method for MGIT Protocol, as described by the Dr. Angelo Izzo Lab, Colorado State University 2020

Samples prepared by Dobos Lab. 2/21/2020 – Samples received from Dobos Lab Samples prepared for MGIT culturing and Petroff-Hausser counting. 2/24/2020 – Samples collected for Petroff-Hausser by placing an aliquot into formalin. Microscope examination revealed the preparations were very clumpy and very difficult to count. 2/25/2020 – The samples were then re-assessed after sonication for 3 mins and vortexing for 30 sec (2 times) for MGIT and Petroff-Hausser counting. Microscope examination revealed the preparations were still very clumpy and very difficult to count. This may be the result of the treatment that attenuates the organism.

MGIT Results MGIT is used for the detection of mycobacteria. The BACTEC MGIT contains modified Middlebrook 7H9 Broth base with OADC enrichment and PANTA antibiotic mixture (polymyxin B, amphotericin B, nalidixic acid, trimethoprim and azlocillin). A fluorescent compound is embedded in silicone on the bottom of each of the tubes, which is sensitive to the presence of oxygen dissolved in the broth. Initially, the large amount of dissolved oxygen quenches the emissions from the compound and little fluorescence can be detected. Later, actively respiring microorganisms consume the oxygen and allow the fluorescence to be detected. The system monitors the tubes for increasing fluorescence. Analysis of the fluorescence is used to determine if the tube is instrument-positive; i.e., the test sample contains viable organisms. Culture tubes which remain negative for a minimum of 42 days.

APPENDIX B

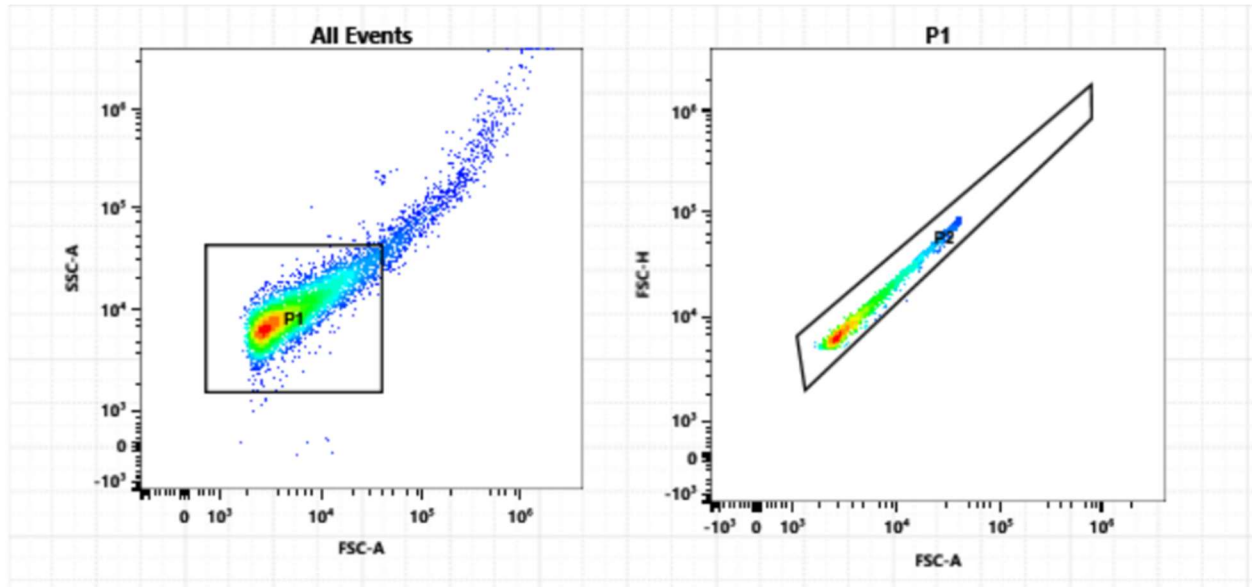


Figure B1 (above). Example of flow cytometry doublet discrimination gating used phase out aggregates or clumps which may potentially bias results

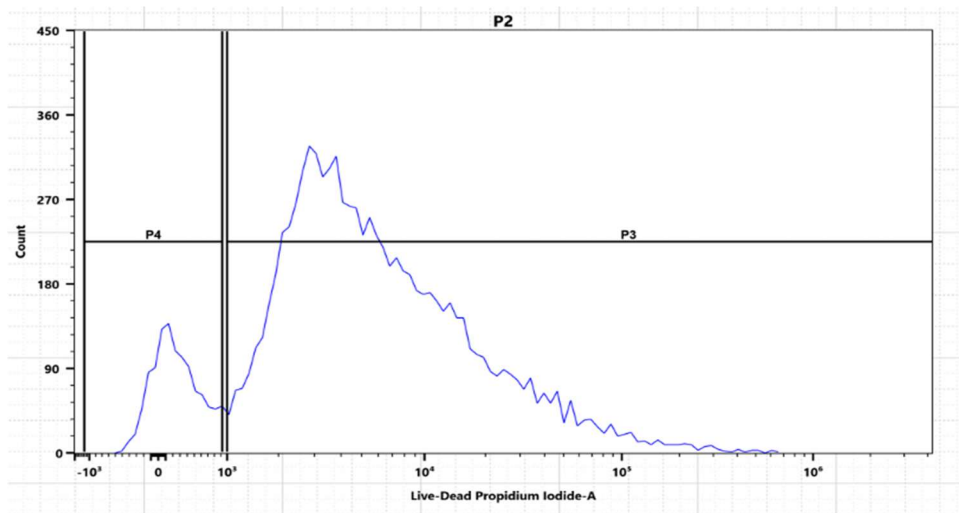
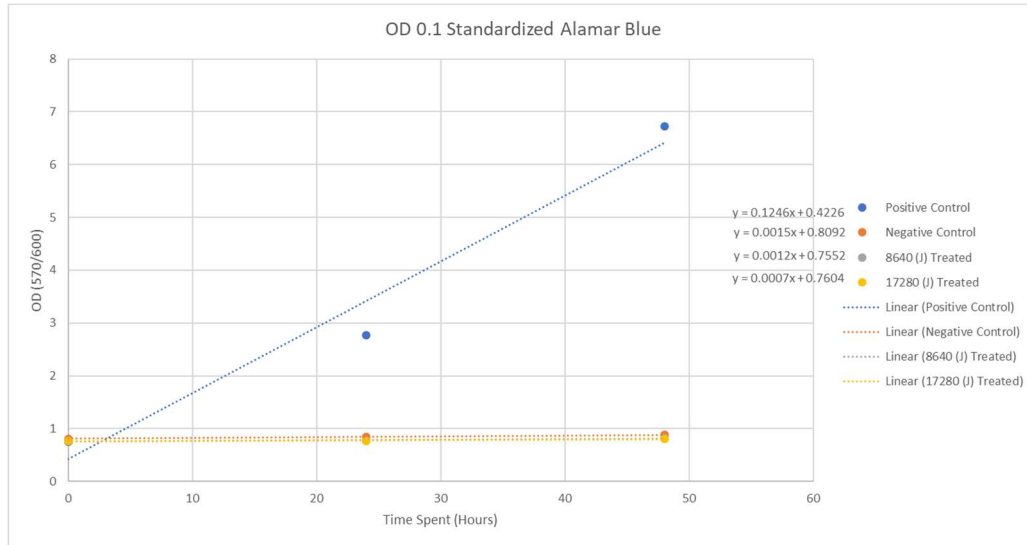
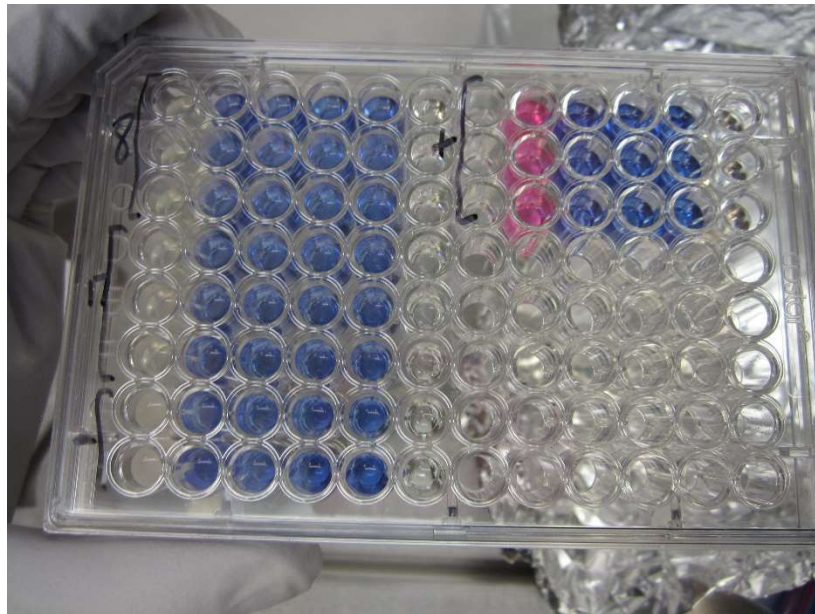


Figure B2 (above). An example of flow cytometry gating based on live-dead stained controls. Gate P4 contains live unstained cells, also based on reference group. Gate P3 contains dead stained cells, which fluoresce in red.

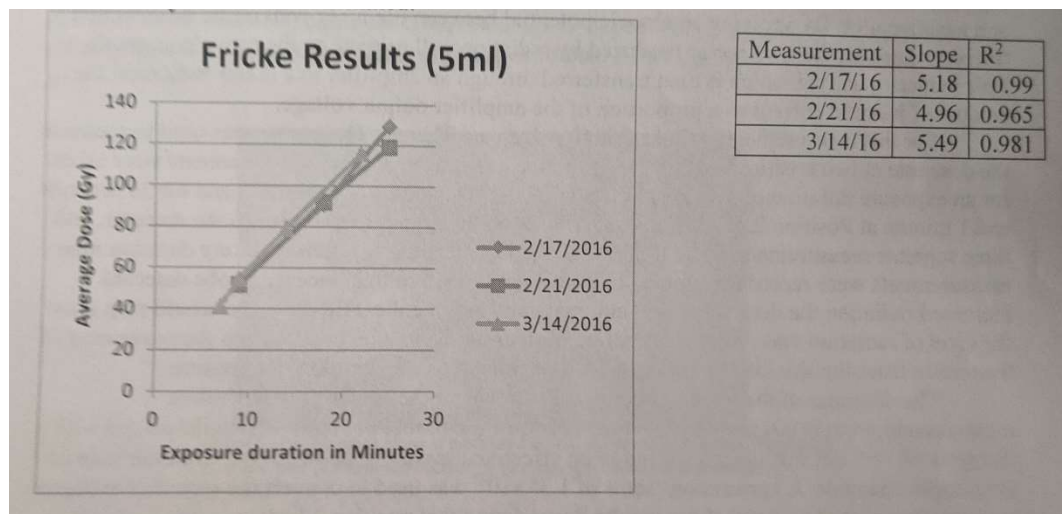
APPENDIX C



Supplementary Figure 1A (above). Nearly a 100 fold increase in growth curve slope observed in positive control compared to treated *Mtb* samples. No observable resazurin reduction in either 8640J, nor 17280J treated *Mtb* over the span of 48h, compared to positive control.



Supplementary Figure 1B (above). Bracket labeled “8” represents colorimetric change over the span of 48h in 8,640J treated *Mtb*. “17” represents the same for the 17,280J treated samples, “-“ for the negative control, and “+” for the *Mtb* positive control.

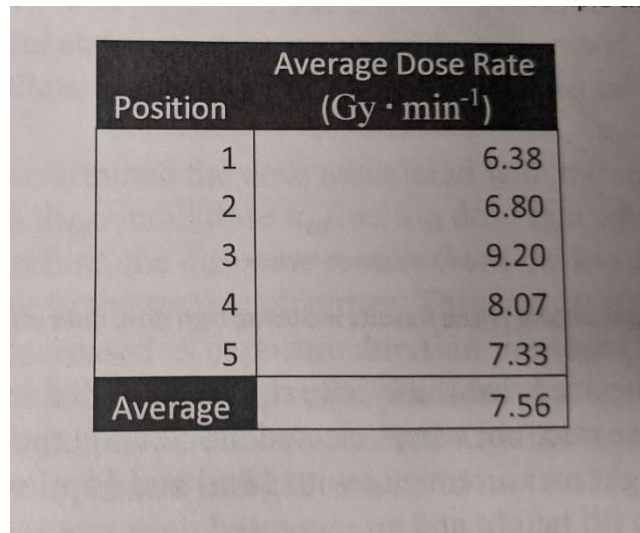


Supplementary Figure 2A (above). Fricke solution was prepared and treated at labeled exposure times to generate predictive curves. Fricke solution was measured at 303 nm, and temperature variance was taken into consideration when calculating for the dose¹⁹.

Table 1. Ion Chamber Results

Position	Exposure Duration (minutes)	Total Dose (Gy)	Dose rate (Gy·min ⁻¹)
1	0.51	3.47	6.80
	1.01	6.79	6.72
	3.01	20.13	6.69
2	0.51	4.06	7.96
	1.01	7.87	7.79

Supplementary Figure 2B (above). Two positions in the chamber were considered. Probe began measurements as soon as radiation was detected, and concluded as soon as radiation was reduced. Biases of -300, 150 and 300 Volts were used, with three measurements at each bias.



Position	Average Dose Rate (Gy · min ⁻¹)
1	6.38
2	6.80
3	9.20
4	8.07
5	7.33
Average	7.56

Supplementary Figure 2C (above). Average dose rates across positions in the thermoluminescent dosimeter. Some variation in dose-rate based on positions was noted.

Supplementary Table 1 (below). Treated H37Rv *Mtb* in MGIT duplicates (a and b). Sample H37Rv 8640 J a returned a time-to-positive result suggesting viable bacteria. This was streaked on 7H11 agar, consequently, and growth was observed within 3 days. Organism was acid-fast positive and gram variable.

Sample	Date in MGIT	TTP (hours)
H37Rv Untreated Control a	2/21/20	72
H37Rv Untreated Control b	2/21/20	73
H37Rv 8640 J a	2/21/20	436
H37Rv 8640 J b	2/21/20	0
H37Rv 17280 J a	2/21/20	0
H37Rv 17280 J b	2/21/20	0
H37Rv Untreated Control a Sonicate/Vortex	2/25/20	79
H37Rv Untreated Control a Sonicate/Vortex	2/25/20	74
H37Rv 8640 J a Sonicate/Vortex	2/25/20	0
H37Rv 8640 J b Sonicate/Vortex	2/25/20	0
H37Rv 17280 J a Sonicate/Vortex	2/25/20	0
H37Rv 17280 J b Sonicate/Vortex	2/25/20	0